Hindawi
Journal of Applied Mathematics
Volume 2023, Article ID 7104852, 32 pages
https://doi.org/10.1155/2023/7104852

Research Article

A Novel Multivariate Spectral Local Quasilinearization Method (MV-SLQLM) for Modelling Flow, Moisture, Heat, and Solute Transport in Soil

Elias Mwakilama,[1,2] **Vusi Magagula**,[3] **and Duncan Gathungu**[4]

[1]*Department of Mathematics, Pan African University Institute for Basic Sciences Technology and Innovation (PAUISTI), Nairobi, Kenya*
[2]*Department of Mathematical Sciences, University of Malawi, Zomba, Malawi*
[3]*Department of Mathematics, University of Eswatini, Kwaluseni, Matsapha, Eswatini*
[4]*Department of Pure & Applied Mathematics, Jomo Kenyatta University of Agriculture & Technology, Nairobi, Kenya*

Correspondence should be addressed to Elias Mwakilama; mwakilama.elias@students.jkuat.ac.ke

Received 18 July 2022; Revised 5 February 2023; Accepted 18 February 2023; Published 15 March 2023

Academic Editor: Theodore E. Simos

Copyright © 2023 Elias Mwakilama et al. This is an open access article distributed under the Creative Commons Attribution License, which permits unrestricted use, distribution, and reproduction in any medium, provided the original work is properly cited.

Conventionally, the problem of studying the transport of water, heat, and solute in soil or groundwater systems has been numerically solved using finite difference (FD) or finite element (FE) methods. FE methods are attractive over FD methods because they are geometrically flexible. However, recent studies demonstrate that spectral collocation (SC) methods converge exponentially faster than FD or FE methods using a few grid points or on coarse grids. This work proposes and applies a multivariate spectral local quasilinearization method (MV-SLQLM) to model the transportation and interaction of soil moisture, heat, and solute concentration in a nonbare soil ridge. The MV-SLQLM uses a quasilinearization method (QLM) to linearize any nonlinear equations and then employs a local linearization method (LLM) to decouple the linearized system of PDEs to form a sequence of equations that are solved in a computationally efficient manner. The MV-SLQLM is thus an extension of the bivariate spectral local linearization method (BI-SLLM) that fails to deal with a 2D problem and is a modification of the MV-SQLM whose efficiency is compromised when operating on high dense solution matrices. We use the residual error norms of the difference between successive iterations to affirm convergence to the expected solution. To illustrate the application and check the solution accuracy, we conduct systematic analyses of the effect of model parameters on distribution profiles. Findings are in good agreement with theory and literature, thereby revealing suitability of the MV-SLQLM to solve coupled nonlinear PDEs with environmental fluid dynamics applications.

1. Introduction

The problem of modelling the transport and interaction of heat and mass in porous media is of interest to the extent that there is a considerable body of work on analytical, semianalytical, and numerical solutions. Because of their ease of use and low costs at implementation, analytical and semianalytical solutions are considered efficient tools for modelling the fate and transport of heat, water, or contaminants in soil or groundwater systems. Among others [1–3], Shao et al. [4] derived analytical solutions for heat transport equations in soil media. Including [5, 6], Chen et al. [7] proposed analytical solutions to linearized Richards equations for describing infiltration. Sanskrityayn et al. [8] and other studies [9–18] provided analytical solutions to modelling the transport of contaminants in soil and groundwater systems. Other studies [19–21] proposed analytical solutions to solute and water transport equations for verifying numerical solvers. Gao et al. [22] and others [23–25] employed semianalytical solutions to model the transport of solutes and water in soil and aquifers. However, the main limitation with analytical and semianalytical solutions is their inability

to handle complex nonlinear models. Moreover, besides a few citable examples, many analytical tools are not multidimensional and do not consider interaction. Numerical models can handle such complexity but at the expense of defining several parameters that are often unknown, leading to model outputs that are highly uncertain [9]. In addition, numerical solutions have natural approximation errors, can be computationally demanding, and may generate very different results using the same input parameters [9].

Nonetheless, several numerical solutions have been proposed to model heat, water, and solute transfer in porous media using finite difference (FD), finite volume (FV), or finite element (FE) methods. The solutions are problem-specific or as general commercial software [26]. Ehrhardt and Mickens [27] and Wang and Roeger [28] proposed nonstandard FD schemes to solve convection-diffusion equations with constant coefficients and convection-diffusion-reaction equations. Soko et al. [29] studied the inverse problem of identifying multiple pollution sources in groundwater systems using a FV method. Noborio et al. [30, 31] developed a two-dimensional (2D) Galerkin FE model for water, heat, and solute transport in soil ridge. Benjamin et al. [32] studied the effect of ridge size and geometry on simulated water and heat transport in soil ridge using a FE model. Baghlani and Nikzad [33] proposed a FD-differential quadrature method for solving 2D unsaturated water flow. Juncu et al. [34] proposed a nonlinear multigrid FD method (FDM) for the numerical solution of the unsaturated flow equation in 2D. Abbas et al. [35] studied a Darcy-Brinkman-Forchheimer model for the laminar natural convection in porous media using a FE method (FEM). Kelleners et al. [36] proposed a FE numerical model of coupled water flow and heat transport in soil and snow. Bennett [37] proposed a FD scheme to solve a Richards' equation. Reichardt and Timm [38] described water redistribution after infiltration into the soil using a FE tool. Ren et al. [39] investigated the effects of temperature gradient on soil water-salt transfer with evaporation using an FD model. Cimolin and Discacciati [40] studied the Navier-Stokes/Forchheimer model for infiltration through porous media using FE. Fujisawa and Murakami [41] employed FEM to numerically analyze coupled flows in porous and fluid domains using the Darcy-Brinkman equations. Celia et al. [42] proposed a general mass-conservative FE numerical solution coupled with Picard iteration for the unsaturated flow equation. Using FEM, Li et al. [43] proposed a numerical homogenization of the Richards equation for unsaturated water flow through heterogeneous soils. Šimunek et al. [44] proposed an HYDRUS model for simulating the movement of water, heat, and multiple solutes in variably saturated media. Fujimaki [45] and Watanabe [46] applied the Hydrus to study irrigation amounts and model water and heat flow in a directionally frozen silt soil, respectively. Haile [47] proposed a VS2DRR FE-based tool to model the transport of reactive contaminants in the vadose zone.

In spite of the aforementioned FD, FV, or FE numerical applications, one major setback with the FD methods is their demand for several or fine grid points to generate approximate solutions of quadratic convergence [48]. Although the FE methods are geometrically flexible and therefore attractive over FD or FV methods [30], classical FE mesh needs to be fine to model inhomogeneity surface material accurately [49]. Consequently, in both FD and FE methods, demand for fine meshes implies excessive use of high number of elements and costly computational means. Despite some advances in the performance of FE methods, through use of h-p or Galerkin versions [50, 51], the development of alternative numerical schemes for efficient and accurate heat and mass transfer analysis remains a subject of interest.

Spectral methods have emerged as attractive numerical techniques in Engineering and Science [52–55]. As demonstrated on various theoretical diffusion-reaction or advection-diffusion problems [56–58], spectral collocation methods (SCM) are more efficient than FD or FE methods. Unlike the FDM and FEM, the SCM converge exponentially fast using a few grid points and on coarse grids at a minimal computational cost [59]. Motsa [60] developed a new spectral local linearization method (SLLM) for solving nonlinear boundary layer flow problems. Later, the SLLM was extended to a BI-SLLM [61]. Thumma and Magagula [62] studied the transient electromagnetohydrodynamic radiative squeezing flow between two parallel Riga plates using the SLLM. Motsa [63] presented and compared the spectral relaxation method (SRM) and spectral local quasilinearization method (SQLM) for solving unsteady boundary layer flow problems. Ansari et al. [64] studied the Jeffrey nanofluid flow near a Riga plate using the SQLM. Motsa [63] and Magagula et al. [65] proposed a bivariate-SQLM (BI-SQLM) to solve nonlinear PDEs. Jamil et al. [66] studied the unsteady MHD micropolar-nanofluids with homogeneous-heterogeneous chemical reactions over a stretching surface using the BI-SLLM. Since both BI-SQLM and BI-SLLM face challenges with problems of large time scales, Motsa et al. [67] and Magagula et al. [68] proposed the nonoverlapping multidomain spectral collocation methods, i.e., multidomain BI-SLLM [69] and multidomain BI-SQLM [65, 70]. Later, Mkhatshwa et al. [71] proposed an overlapping multidomain spectral method to study conjugate problems of conduction and MHD free convection flow of nanofluids over flat plates. Dlamini and Magagula [72] proposed a multivariate SQLM (MV-SQLM) to solve 2D Burger's equations. Lekoko et al. [73] and Goqo et al. [74] applied the MV-SQLM to analyze pressure and heat distribution in a filter chamber and to study heat and mass transfer in a porous media saturated with nanofluid, respectively. Related to the MV-SQLM is the trivariate spectral collocation method (TV-SCM) proposed by Samuel and Motsa [75]. The MV-SQLM is an extension of the BI-SQLM as the latter does not handle 2D problems. However, the BI-SQLM and MV-SQLM generate more dense solution matrices when solving a coupled system of ODEs or PDEs, thereby compromising numerical efficiency. The BI-SLLM, however, employs the LLM to decouple the system and iteratively solve the problem on low-dense solution matrices, but for 1D problems.

Despite the case, performance analysis of the previous spectral variants has depended heavily upon theoretical or practical nanofluid type of problems [59], whose medium of transmission differs from that of soil. Soil structure presents complex modelling processes that lead to highly

coupled flow governing equations. In this work, we propose and apply a multivariate spectral local quasilinearization method (MV-SLQLM), extending the BI-SLLM and modifying the MV-SQLM, to model the transport and interaction of heat and mass in a 2D homogeneous porous medium. The MV-SLQLM uses the quasilinearization method (QLM) of Bellman et al. [76] to linearize the nonlinear equations and the local linearization method (LLM) [60, 61] to decouple the system and efficiently solve the problem on low-dense matrices. The proposed solution method is motivated by a practical problem of understanding transport and interaction of soil moisture, soil temperature, and solute concentration in a soil ridge with water in the furrows. Previously, Benjamin et al. [32] investigated the bare ridge tillage (height) effect on the simulated water and heat transport, disregarding presence of solute. Noborio et al. [30] studied the interaction of water, heat, and solute in furrow-irrigated soil, but with a focus on the effect of bare soil ridge surface and furrow. Our work assumes nonbare soil ridge to include the effect of plant-root uptake activity. Using the proposed MV-SLQLM, this study generates knowledge of the simultaneous distribution and interaction of soil water, moisture, heat, and solute in a nonbare soil ridge, useful for the proper management of ridge-tillage soil field to enhance crop production.

The rest of the paper is organized as follows: in Section 2, we present the investigated domain and the governing equations. In Section 3, we describe the solution method, error, and stability analysis and illustrate how the method is employed to solve the mentioned problem. Simulation results are presented and discussed in Section 4, along with convergence rate of the proposed method. Finally, Section 5 summarizes and concludes the current study.

2. Investigated Domain and Governing Equations

Guided by the characteristics of natural convection flow in a homogeneous porous medium, this study considers a problem of environmental application that describes the transport and interaction of soil moisture, heat, and solute concentration in a nonbare soil ridge when liquid water is present in the furrows (Figure 1). Knowledge of interactive transport mechanisms inside a nonbare soil ridge is vital to agronomists and environmental researchers for upholding good environmental conditions (SDG 13), promoting life on land (SDG 15), and ensuring food secure nations (SDG 2). Figure 1(a) describes the study domain.

Naturally, a soil ridge resembles an experimental soil column (porous pack), heated at the top and cooled at the bottom so that it also contains a vapor zone near top surface, a liquid zone at the bottom, and a two-phase zone in between (Figure 1(b), adapted from [77]). Hence, the model under consideration is that of an unsteady natural convection flow in a porous medium of nonbare ridge such that equations describing transport of moisture and solute concentration are coupled with sink terms. Further, it is assumed that buoyancy forces are present due to temperature and concentration variation of the fluid flow. The continuity equation (1) and equations governing flow, momentum, energy, moisture, and concentration are (2)–(6) [78]

$$\frac{\partial u}{\partial x} + \frac{\partial w}{\partial z} = 0, \tag{1}$$

$$\rho\left(\frac{\partial u}{\partial t} + u\frac{\partial u}{\partial x} + w\frac{\partial u}{\partial z}\right) = \mu\left(\frac{\partial^2 u}{\partial x^2} + \frac{\partial^2 u}{\partial z^2}\right) - \frac{\mu}{k}u - \frac{\rho F u^2}{\sqrt{k}}, \tag{2}$$

$$\begin{aligned}\rho\left(\frac{\partial w}{\partial t} + u\frac{\partial w}{\partial x} + w\frac{\partial w}{\partial z}\right) &= -\frac{\partial P}{\partial z} + \mu\left(\frac{\partial^2 w}{\partial z^2} + \frac{\partial^2 w}{\partial z^2}\right) \\ &\quad - \frac{\mu}{k}w - \frac{\rho F w^2}{\sqrt{k}} + (\rho g)[\beta(T - T_0) + \beta^*(C - C_0)],\end{aligned} \tag{3}$$

$$\begin{aligned}&\widehat{C}_A\frac{\partial T}{\partial t} + \left(\widehat{C}_w q_w + \widehat{C}_v q_v\right)\frac{\partial T}{\partial x} + \left(\widehat{C}_w q_w + \widehat{C}_v q_v\right)\frac{\partial T}{\partial z} \\ &\quad = \widehat{\lambda}\left(\frac{\partial^2 T}{\partial x^2} + \frac{\partial^2 T}{\partial z^2}\right) - L_0\left(\frac{\partial q_v}{\partial x} + \frac{\partial q_v}{\partial z}\right) \\ &\qquad - \mu\left(\frac{\partial q_w}{\partial x}\right)^2 + \varsigma(T - T_0),\end{aligned} \tag{4}$$

$$\begin{aligned}&\frac{\partial \theta}{\partial t} - \frac{\partial}{\partial x}\left(D_\theta\frac{\partial \theta}{\partial x} + D_T\frac{\partial T}{\partial x}\right) - \frac{\partial}{\partial z}\left(D_\theta\frac{\partial \theta}{\partial z} + D_T\frac{\partial T}{\partial z}\right) \\ &\quad = \frac{\partial K_\theta}{\partial z} - S(z,t),\end{aligned} \tag{5}$$

$$\begin{aligned}&(\rho_b\kappa_d + \theta_w)\frac{\partial C}{\partial t} + \left(q_x\frac{\partial C}{\partial x} + q_z\frac{\partial C}{\partial z}\right) + \eta_w'(\theta_w C + \rho_b C_a) - \zeta_s C_s \\ &\quad = \frac{\partial}{\partial x}\left(\theta_w D\frac{\partial C}{\partial x} + D_{\mathrm{TM}}\frac{\partial^2 T}{\partial x}\right) + \frac{\partial}{\partial z}\left(\theta_w D\frac{\partial C}{\partial z} + D_{\mathrm{TM}}\frac{\partial^2 T}{\partial z}\right),\end{aligned} \tag{6}$$

where u and w are velocity components, and P is the pressure of the fluid; ρ and μ are density and viscosity of the fluid, respectively; and F and k are, respectively, the inertia resistance coefficient and the permeability coefficient. Following the Darcy-Boussinesq approximation assumption [79] on the vertical flow, g is the force due to gravity, and β and β^* are, respectively, volumetric coefficients of expansion of heat and contaminants. The terms T_0 and C_0 in equation (3) represent medium surface temperature and concentration, respectively. The presence of sink terms, $S(z,t)$ in equation (5) and C_s in equation (6), mimics the plant-root uptake activity due to the nonbare ridge surface assumption.

In equation (4), $\widehat{C}_A = \widehat{C}_s + L_0\partial\theta_v/\partial t$ is the apparent heat capacity or the heat flow retardation factor [46], where $\widehat{C}_s = (\rho c_p)_s$, $\widehat{C}_w = (\rho c_p)_l$, and $\widehat{C}_v = (\rho c_p)_v$ are, respectively, the volumetric heat capacities of the porous medium, the liquid phase, and the vapor phase; q_w and q_v are the liquid flux and vapor flux densities, respectively; $\widehat{\lambda}$ is the apparent thermal conductivity of soil; and L_0 is the volumetric latent heat of vaporization of liquid water. Otherwise, in equation (5), D_θ, D_T, and K_θ are, respectively, unsaturated moisture

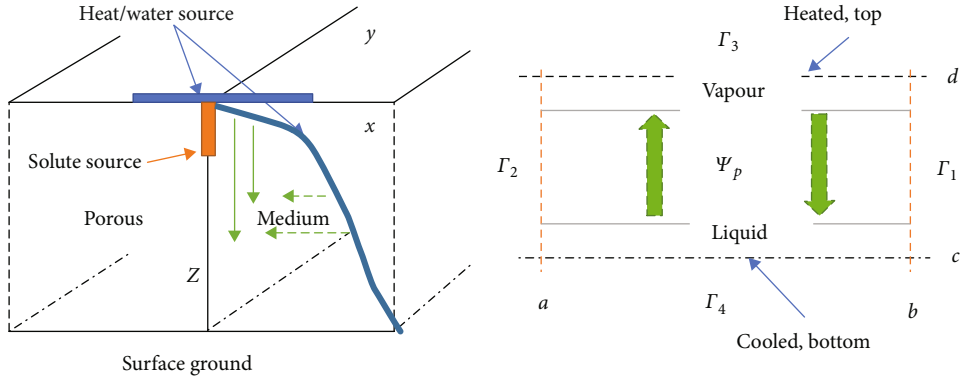

(a) Study domain (b) Porous pack with boundaries

FIGURE 1: Schematic configuration of the homogeneous porous media.

diffusivity, coefficient of Soret effect of temperature in moisture flux, and unsaturated hydraulic conductivity.

In equation (6), θ_w is volumetric water content $(-)$; D is the hydrodynamic dispersion coefficient $(\mathrm{m^2 s^{-1}})$; q is the Darcian fluid flux density $(\mathrm{m^3 m^{-2} s^{-1}})$; ρ_b is the soil bulk density $(\mathrm{Kgm^{-3}})$; C_a is the concentration of contaminants adsorbed onto the solid surface $(\mathrm{mgKg^{-1}})$; η'_w is the first-order reaction rate coefficient $(\mathrm{s^{-1}})$; and S_c is the contaminant sink term $(\mathrm{Mgm^{-3} s^{-1}})$. Additionally, k_d is the distribution coefficient for linear adsorption process $(\mathrm{m^3 Mg^{-1}})$, ζ_s is the volumetric flux of water per unit volume of soil matrix $(\mathrm{s^{-1}})$; C_s is the concentration of contaminants at sink; $R_m = (\rho_b \kappa_d + \theta_w)$ is the soil matrix retardation factor $(-)$; D_{TM} is the thermal gradient diffusion coefficient $(\mathrm{m^2 (s^\circ C)^{-1}})$; and q_x and q_z are, respectively, seepage velocity components in the horizontal and vertical directions.

The initial and boundary conditions to (2)–(6) are [78]

$$\vec{u}(x,z,0) = 0,\ T(x,z,0) = T_i, \theta(x,z,t) = \theta_0 C(x,z,0) = C_i, \tag{7a}$$

$$u(a,z,t) = U_{wm}, w(a,z,t) = 0, u(b,z,t) = U_{wm}, w(b,z,t) = 0, \tag{7b}$$

$$u(x,c,t) = 0, w(x,c,t) = 0, u(x,d,t) = 0, w(x,d,t) = V_{wm}, \tag{7c}$$

$$\left.\frac{\partial T}{\partial x}\right|_a = q', \left.\frac{\partial T}{\partial x}\right|_b = q', T(x,c,t) = 0, T(x,d,t) = (T_0 - T_i), \tag{7d}$$

$$\left.\frac{\partial \theta}{\partial x}\right|_a = E_x, \left.\frac{\partial \theta}{\partial x}\right|_b = E_x, \theta(x,c,t) = 0, \theta(x,d,t) = \theta_r, \tag{7e}$$

$$\left.\frac{\partial C}{\partial x}\right|_a = 0, \left.\frac{\partial C}{\partial x}\right|_b = 0, C(x,c,t) = 0, C(x,d,t) = 0. \tag{7f}$$

Applying the following nondimensional variables

$$x^* = \frac{x}{L}, z^* = \frac{z}{L}, \phi = \frac{d}{L}, u^* = \frac{u}{U_0 \phi}, w^* = \frac{w}{U_0 \phi}, q^* = \frac{q}{U_0 \phi}, P^* = \frac{P}{\rho U_0^2}, \tag{8}$$

$$T^* = \frac{(T - T_i)}{(T_0 - T_i)}, C^* = \frac{(C - C_i)}{(C_0 - C_i)}, t^* = \frac{t}{L/U_0}, \tag{9}$$

we obtain (upon dropping the asterisk) the dimensionless equations [78]

$$\frac{\partial u}{\partial t} + \phi u \frac{\partial u}{\partial x} + \phi w \frac{\partial u}{\partial z} = \frac{1}{\mathrm{Re}}\left(\frac{\partial^2 u}{\partial x^2} + \frac{\partial^2 u}{\partial z^2}\right) - \frac{u}{\mathrm{Re} \cdot \Lambda} - \frac{F^*}{\mathrm{Re}} u^2, \tag{10}$$

$$\frac{\partial w}{\partial t} + \phi u \frac{\partial w}{\partial x} + \phi w \frac{\partial w}{\partial z} = -\frac{1}{\phi}\frac{\partial P}{\partial z} + \frac{1}{\mathrm{Re}}\left(\frac{\partial^2 w}{\partial x^2} + \frac{\partial^2 w}{\partial z^2}\right) - \frac{w}{\mathrm{Re} \bullet \Lambda} - \frac{F^*}{\mathrm{Re}} w^2 + \frac{1}{\phi}\left(\frac{Gr^T + Gr^C}{\mathrm{Re}^2}\right), \tag{11}$$

$$\frac{\partial T}{\partial t} + \varrho_1 \phi \left(q_x \frac{\partial T}{\partial x} + q_z \frac{\partial T}{\partial z}\right) = \frac{1}{\mathrm{Pr} \bullet \mathrm{Re}}\left(\frac{\partial^2 T}{\partial x^2} + \frac{\partial^2 T}{\partial z^2}\right) - \phi \frac{Ec}{\mathrm{Re}} \varrho_2 L_0 \left(\frac{\partial q_v}{\partial x} + \frac{\partial q_v}{\partial z}\right) + \frac{\phi^2 Ec}{\mathrm{Re}}\left(\frac{\partial q_w}{\partial x}\right)^2 + \frac{\delta_1}{\mathrm{Pr} \bullet \mathrm{Re}} T, \tag{12}$$

$$R_m \frac{\partial C}{\partial t} + \phi\left(q_x \frac{\partial C}{\partial x} + q_z \frac{\partial C}{\partial z}\right) = \frac{\theta_w}{Pe}\left(\frac{\partial^2 C}{\partial x^2} + \frac{\partial^2 C}{\partial z^2}\right) + \bar{\zeta}\left(\frac{\partial^2 T}{\partial x^2} + \frac{\partial^2 T}{\partial z^2}\right) + \varrho_3 C + \varrho_4 C_a + \varrho_5, \tag{13}$$

where $\mathrm{Pr} = (\mu c_p)/k$ is the Prandtl number; $\mathrm{Re} = (\rho U_0 L)/\mu$ is the Reynolds number; $Ec = U_0^2/c_p(T_0 - T_i)$ is the Eckert number; $F^* = \phi\,\mathrm{Re}\,F/\sqrt{\Lambda}$ is the Forchheimer number, where Λ is the Darcy number; $Gr^T = (g\beta(T_0 - T_i)L^3\rho^2)/\mu^2$ is the Grashof number due to soil temperature; $Gr^C = (g\beta(C_0 - C_i)L^3\rho^2)/\mu^2$ is the Grashof number due to soil concentration; and $\mathrm{Pe} = U_0 L/D$ is the Peclet number.

In addition, $\rho_1 = (\rho c_p)_w/(\rho_b c_p)_s$ is the heat capacity ratio parameter, $\delta_1 = \varsigma/\widehat{\lambda}$ is the heat generation/absorption parameter, $\bar{\zeta} = (D_{\mathrm{TM}}(T_0 - T_i)/(U_0 L)$ is the thermophoresis parameter, $\rho_2 = L/U_0$ is the characteristic time, $\rho_3 = (\eta_w' \theta_w L)/U_0$ is the chemical reaction parameter, $\rho_4 = (\eta_w' \rho_b L)/(U_0(C_0 - C_i))$ is the sorption parameter, $\rho_5 = \zeta_s L C_s/(U_0(C_0 - C_i))$ is the chemical sink parameter, and $R_m = 1 + (\rho_b \kappa_d)/\theta_w$ is the soil matrix retardation factor.

Equation (5) is highly nonlinear and degenerate because of K_θ and D_θ that also depend on the field variable θ. For simplicity, we first rewrite equation (5) as

$$\frac{\partial \theta}{\partial t} = D_T\left(\frac{\partial^2 T}{\partial x^2} + \frac{\partial^2 T}{\partial z^2}\right) + D_\theta\left(\frac{\partial^2 \theta}{\partial x^2} + \frac{\partial^2 \theta}{\partial z^2}\right) - \frac{\partial K_\theta}{\partial z} + \frac{\partial \theta_z}{\partial t}, \tag{14}$$

where $\partial\theta_z/\partial t$ replaces the sink term $S(z,t)$ to describe the "rate of moisture uptake by the plant root in the z-direction" only. Then, using the relation [20]

$$\frac{\partial K_\theta}{\partial z} = \frac{K_s}{(\theta_s - \theta_r)}\left(\frac{\partial \theta}{\partial z}\right), \tag{15}$$

equation (14) is rewritten as

$$\frac{\partial \theta}{\partial t} = D_T\left(\frac{\partial^2 T}{\partial x^2} + \frac{\partial^2 T}{\partial z^2}\right) + D_\theta\left(\frac{\partial^2 \theta}{\partial x^2} + \frac{\partial^2 \theta}{\partial z^2}\right) - \frac{K_s}{(\theta_s - \theta_r)}\left(\frac{\partial \theta}{\partial z}\right) + \frac{\partial \theta_z}{\partial t}. \tag{16}$$

Using the expression [34]

$$\theta^* = \left(\frac{\theta - \theta_r}{\theta_s - \theta_r}\right), \tag{17}$$

where θ^* is the "relative water/moisture content," and the following nondimensional variables

$$x^* = \frac{x}{d}, z^* = \frac{z}{L}, T^* = \frac{(T - T_i)}{(T_0 - T_i)}, t^* = \frac{D_\theta t}{L^2}, \tag{18}$$

lead to a simplified and nondimensional moisture (normalized) equation [78]

$$R_n \frac{\partial \theta}{\partial t} = \frac{\Delta T}{\Delta \theta} Le'\left(\frac{\partial^2 T}{\partial x^2} + \frac{\partial^2 T}{\partial z^2}\right) + \left(\frac{\partial^2 \theta}{\partial x^2} + \frac{\partial^2 \theta}{\partial z^2}\right) - \delta_2\left(\frac{\partial \theta}{\partial z}\right), \tag{19}$$

where $R_n = 1 + \partial\theta_z/\partial\bar{u}$ is the moisture retardation factor; $Le' = D_T/D_\theta$ is the Lewis number or "reciprocal" Luikov number; $\delta_2 = (K_s L)/D_\theta(\theta_s - \theta_r)$ is the ratio of "apparent" diffusion coefficients; and $\Delta T = T_0 - T_i$.

The dimensionless initial and boundary conditions are [78]

$$\vec{u}(x,z,0) = 0, T(x,z,0) = T_i, \theta(x,z,t) = \theta_0, C(x,z,0) = C_i, \tag{20a}$$

$$u(a,z,t) = \frac{U_{wm}}{U_0\phi}, w(a,z,t) = 0, u(b,z,t) = \frac{U_{wm}}{U_0\phi}, w(b,z,t) = 0, \tag{20b}$$

$$u(x,c,t) = 0, w(x,c,t) = 0, u(x,d,t) = 0, w(x,d,t) = \frac{V_{wm}}{U_0^2\phi}, \tag{20c}$$

$$\left.\frac{\partial T}{\partial x}\right|_a = \frac{q'd}{(T_0 - T_i)}, \left.\frac{\partial T}{\partial x}\right|_b = \frac{q'd}{(T_0 - T_i)}, T(x,c,t) = \frac{-T_i}{(T_0 - T_i)}, T(x,d,t) = \frac{(T_0 - 2T_i)}{(T_0 - T_i)}, \tag{20d}$$

$$\left.\frac{\partial C}{\partial x}\right|_a = 0, \left.\frac{\partial C}{\partial x}\right|_b = 0, C(x,c,t) = 0, C(x,d,t) = 1, \tag{20e}$$

$$\left.\frac{\partial \theta}{\partial x}\right|_a = \frac{E_x d}{(\theta_s - \theta_r)}, \left.\frac{\partial \theta}{\partial x}\right|_b = \frac{E_x d}{(\theta_s - \theta_r)}, \theta(x,c,t) = 0, \theta(x,d,t) = \frac{(\theta_0 - \theta_r)}{(\theta_s - \theta_r)}. \tag{20f}$$

Since it is generally difficult to obtain estimates of Darcy flux densities for the investigated domain, the soil heat (12) and contaminant (13) equations are instead coupled to the flow equations ((10) and (11)). To achieve this, we first consider the expression of Darcy flux density $\vec{q}$ [80]

$$\vec{q} = -\frac{K_h}{\phi_e}\frac{dh}{dl}, \tag{21}$$

where h is the hydraulic head (m), ϕ_e is the effective porosity, and l is the single direction distance over which the measured change in the hydraulic head is measured (m). Using the definitions of moisture specific capacity $C(h) = d\theta/dh$ and unsaturated moisture diffusivity $D_\theta = K_h/C(h)$ yields a new expression

$$D_\theta = K_h \frac{dh}{d\theta}. \tag{22}$$

Combining equations (21) and (22) yields

$$\vec{q} = -\frac{D_\theta}{\phi_e}\frac{d\theta}{dl}, \tag{23}$$

such that

$$\frac{\partial \vec{q}}{\partial l} = -\frac{D_\theta}{\phi_e}\frac{\partial^2\theta}{\partial l^2}. \tag{24}$$

Using the relationship between the Darcy flux density $\vec{q}$ and the average seepage velocity $\vec{u}$ [80],

$$\vec{u} = \frac{\vec{q}}{\phi_e}, \tag{25}$$

together with equation (24), we deduce the following expressions;

$$q_x = u\phi_e\,;\, q_z = w\phi_e\,;\, \frac{\partial q}{\partial x} = -\frac{D_\theta}{\phi_e}\frac{\partial^2\theta}{\partial x^2}\,;\, \frac{\partial q}{\partial z} = -\frac{D_\theta}{\phi_e}\frac{\partial^2\theta}{\partial z^2}. \tag{26}$$

Then, using the first two terms of (26), we replace the Darcy flux density components q_x and q_z in equations (12) and (13) with the "average" seepage velocity components u and w, respectively; the solutions of equations (10) and (11), respectively. Consequently, equations (12) and (13) are coupled with equations (10) and (11). In a similar manner, the last two expressions of (26) replace the term $(\partial q/\partial x + \partial q/\partial z)$ in equation (12) to be eloquently coupled with equation (19).

Lastly, the parameters $\varrho_3 = (\eta_w'\theta_w L)/U_0$, $\varrho_4 = (\eta_w'\rho_b L)/(U_0(C_0 - C_i))$, and $\varrho_5 = \zeta_s L C_s/(U_0(C_0 - C_i))$ in equation (13) are further rearranged. Introducing a "one," d/d to the RHS of ϱ_3, results into

$$\varrho_3' = \frac{\eta_w'\theta_w d^2}{\breve{D}}, \tag{27}$$

where $\breve{D} \equiv U_0 d$ is the apparent diffusivity of the porous matrix. Hence, equation (27) is expressed in the form of the Damköhler (Da) number [23]

$$\mathrm{Da} = \frac{k_j b_2^2}{D^*}, \tag{28}$$

when $k_j \equiv \eta_w'$, $b_2 \equiv d$, and $D^* \equiv \breve{D}$, where b, k_j, and D are, respectively, half-fracture aperture length, reaction rate constant, and matrix diffusion coefficient. Hence, the nondimensional parameter ϱ'_3 (equation (27)) is termed "apparent" Damköhler number. In a similar manner, the rearranged forms of ϱ_4 and ϱ_5 are, respectively,

$$\varrho_4' = \frac{\rho_b \kappa_d}{(C_0 - C_i)}\mathrm{Da} \quad \text{and}\, \varrho_5' = \frac{\zeta_s d^2 C_s}{\breve{D}(C_0 - C_i)}, \tag{29}$$

where ϱ_4' in (29) is now called the "weighted" Damköhler number.

3. Derivation of Solution Method

3.1. MV-SLQLM Approximation and Construction in (2 + 1) Dimensions. Suppose we have a general nonlinear PDE of the form

$$\frac{\partial}{\partial t} = \mathscr{F}\left(\frac{\partial^2 u}{\partial x^2}, \frac{\partial^2 u}{\partial z^2}, \frac{\partial u}{\partial x}, \frac{\partial u}{\partial z}, u\right), \tag{30}$$

for $(x, z, t) \in [a, b] \times [c, d] \times [0, T]$, where $\mathscr{F}$ is a nonlinear operator.

To solve equation (30), first, we require the QLM to linearize any nonlinear equations [67]. Then, we approximate the unknown solution $u(x, z, t)$ of each linear equation using the triple Lagrange interpolation functions $L_i(x)$, $L_j(z)$, and $L_k(t)$ at the Chebyshev-Gauss-Lobatto (CGL) collocation points $(\tilde{x}, \tilde{z}, \tilde{t})$ located in the local support domain $[-1, 1]^3$. Like in the generalized differential quadrature (GDQ) method [81], the use of Gauss-Lobatto (GL) rule permits grid points to be located on the boundaries, appropriate for the application of boundary conditions. Moreover, grid points with nonuniform intervals provide more accurate results in the calculation of numerical integrals and derivatives.

As with other related meshless methods [49, 82], accuracy and efficiency of any spectral method depend on the number of nodes (collocation points) in the local support domain. We thus obtain the spectral domain $[-1, 1]^3$ from the original domain $(x, z, t) \in [a, b] \times [c, d] \times [0, T]$ via the linear transformation,

$$\begin{aligned} x &= \frac{1}{2}(b - a)\tilde{x} + \frac{1}{2}(a + b), z \\ &= \frac{1}{2}(d - c)\tilde{z} + \frac{1}{2}(c + d), \text{and } t = \frac{1}{2}\left(\tilde{t} + 1\right), \end{aligned} \tag{31}$$

where [55]

$$\begin{aligned} \{\tilde{x}_i\} &= \left\{\cos\left(\frac{\pi i}{N_x}\right)\right\}_{i=0}^{N_x}, \{\tilde{z}_j\} = \left\{\cos\left(\frac{\pi j}{N_z}\right)\right\}_{j=0}^{N_z}, \{\tilde{t}_k\} \\ &= \left\{\cos\left(\frac{\pi k}{N_t}\right)\right\}_{k=0}^{N_t}, \end{aligned} \tag{32}$$

is the collocation points described by the Chebyshev polynomial $T_N(v)$ of order $N \in \mathbb{N}$,

$$T_N(v) = \cos\left(N \arccos(v)\right). \tag{33}$$

Then, we approximate each function $u(x,z,t)$ by the Chebyshev interpolation $u_N(x,z,t)$, where

$$U_N(x,z,t) = \sum_{k=0}^{N_t}\sum_{j=0}^{N_z}\sum_{i=0}^{N_x} u_{kji}L_k(t)L_j(z)L_i(x), \tag{34}$$

together with the corresponding approximate derivatives at the collocation points,

$$\frac{\partial^n}{\partial x^n}u(\tilde{x}_i,\tilde{z}_j,\tilde{t}_k) = \sum_{r=0}^{N_t}\sum_{q=0}^{N_z}\sum_{p=0}^{N_x} u_{kji}L_r(\tilde{t}_k)L_q(\tilde{z}_j)D_{pi}^{(n)}, \tag{35a}$$

$$\frac{\partial^n}{\partial z^n}u(\tilde{x}_i,\tilde{z}_j,\tilde{t}_k) = \sum_{r=0}^{N_t}\sum_{q=0}^{N_z}\sum_{p=0}^{N_x} u_{kji}L_r(\tilde{t}_k)D_{qj}^{(n)}L_p(\tilde{x}_i), \tag{35b}$$

$$\frac{\partial^n}{\partial t^n}u(\tilde{x}_i,\tilde{z}_j,\tilde{t}_k) = \sum_{r=0}^{N_t}\sum_{q=0}^{N_z}\sum_{p=0}^{N_x} u_{kji}D_{rk}^{(n)}L_q(\tilde{z}_j)L_p(\tilde{x}_i), \tag{35c}$$

where $D_{pi}^{(n)} = L_i^{(n)}(\tilde{x}_i)$, $D_{qj}^{(n)} = L_j^{(n)}(\tilde{z}_j)$, and $D_{rk}^{(n)} = L_k^{(n)}(\tilde{t}_k)$ are, respectively, $(N_x+1)\times(N_x+1)$, $(N_z+1)\times(N_z+1)$, and $(N_t+1)\times(N_t+1)$ Chebyshev differentiation matrices for $i,j,k = 0,1,\cdots,N$.

Further, a Lagrange polynomial of order N, for example, at the Chebyshev-Gauss-Lobatto points $L_i(v)$, is defined as [72]

$$L_i(v) = \frac{(-1)^{i+1}\left(1-v^2\right)T_N'(v)}{\bar{\sigma}_i N^2(v-v_i)}, \quad i = 0,1,2,\cdots,N, \tag{36}$$

where $\bar{\sigma}_i = 1$ for $i = 1,2,\cdots,N-1$, and $\bar{\sigma}_0 = \bar{\sigma}_N = 2$. In addition, the first order Chebyshev differentiation matrix at the collocation points is given by [52, 55]

$$D_{ij}^{(1)} = \begin{cases} \dfrac{\bar{\sigma}_j(-1)^{j+i}}{\bar{\sigma}_i\left(v_j - v_i\right)}, & i \neq j, \\ -\dfrac{v_i}{2\left(1-v_i^2\right)}, & (i=j)\neq 0, N, \\ \dfrac{2N^2+1}{6}, & i,j = 0, \\ \dfrac{2N^2+1}{6}, & i,j = N. \end{cases} \tag{37}$$

For simplicity and efficiency, we express equations (34), (35a), (35b), and (35c) in matrix form, using the Kronecker product, as [72]

$$u(\tilde{x}_i,\tilde{z}_j,\tilde{t}_k) = \left(L(\tilde{t}_k)\otimes L(\tilde{z}_j)\otimes L(\tilde{x}_i)\right)U, \tag{38a}$$

$$\frac{\partial^n}{\partial x^n}u(\tilde{x}_i,\tilde{z}_j,\tilde{t}_k) = \left(L(\tilde{t}_k)\otimes L(\tilde{z}_j)\otimes \vec{D}_x^{(n)}\right)U, \tag{38b}$$

$$\frac{\partial^n}{\partial z^n}u(\tilde{x}_i,\tilde{z}_j,\tilde{t}_k) = \left(L(\tilde{t}_k)\otimes \vec{D}_z^{(n)}\otimes L(\tilde{x}_i)\right)U, \tag{38c}$$

$$\frac{\partial^n}{\partial t^n}u(\tilde{x}_i,\tilde{z}_j,\tilde{t}_k) = \left(\vec{D}_t^{(n)}\otimes L(\tilde{z}_j)\otimes L(\tilde{x}_i)\right)U, \tag{38d}$$

where $U = [u_{000},\cdots,u_{00N_x},\ u_{010},\cdots,u_{01N_x},\cdots,u_{0N_xN_z},\ u_{100},\cdots,u_{N_tN_zN_x}]^T$,

$$L(\tilde{t}_k) = \left[L_0(\tilde{t}_k), L_1(\tilde{t}_k), L_2(\tilde{t}_k),\cdots,L_{N_t}(\tilde{t}_k)\right], \tag{39a}$$

$$L(\tilde{z}_j) = \left[L_0(\tilde{z}_j), L_1(\tilde{z}_j), L_2(\tilde{z}_j),\cdots,L_{N_z}(\tilde{z}_j)\right], \tag{39b}$$

$$L(\tilde{x}_i) = \left[L_0(\tilde{x}_i), L_1(\tilde{x}_i), L_2(\tilde{x}_i),\cdots,L_{N_x}(\tilde{x}_i)\right], \tag{39c}$$

and

$$\begin{aligned} L(\tilde{t}_k)\otimes L(\tilde{z}_j)\otimes L(\tilde{x}_i) = \big[&L_0(\tilde{t}_k)L_0(\tilde{z}_j)L(\tilde{x}_i),\cdots,L_0(\tilde{t}_k)L_{N_z} \\ &\cdot(\tilde{z}_j)L(\tilde{x}_i), L_1(\tilde{t}_k)L_0(\tilde{z}_j)L(\tilde{x}_i),\cdots,L_1 \\ &\cdot(\tilde{t}_k)L_{N_z}(\tilde{z}_j)L(\tilde{x}_i),\cdots,L_{N_t} \\ &\cdot(\tilde{t}_k)L_{N_z}(\tilde{z}_j)L(\tilde{x}_i)\big]. \end{aligned} \tag{40}$$

Third, we formulate the spectral collocated coupled system, defined for each equation, as

$$\tilde{U}^{s+1} = \left\{U^s, W^s, U_x^s, U_{xx}^s, U_z^s, U_{zz}^s, W^{s+1}\right\}, \tag{41a}$$

$$\tilde{W}^{s+1} = \left\{W^s, U^s, W_x^s, W_{xx}^s, W_z^s, W_{zz}^s, U^{s+1}\right\}, \tag{41b}$$

$$\tilde{T}^{s+1} = \left\{T^s, U^s, W^s, T_x^s, T_{xx}^s, T_z^s, T_{zz}^s, \Theta^{s+1}\right\}, \tag{41c}$$

$$\tilde{\Theta}^{s+1} = \left\{\Theta^s, \Theta_x^s, \Theta_{xx}^s, \Theta_z^s, \Theta_{zz}^s, T^{s+1}\right\}, \tag{41d}$$

$$\tilde{C}^{s+1} = \left\{C^s, U^s, W^s, C_x^s, C_{xx}^s, C_z^s, C_{zz}^s, T^{s+1}\right\}. \tag{41e}$$

We apply the LLM algorithm to decouple the spectral collocated system (41a), (41b), (41c), (41d), and (41e) and solve each equation as follows:

(a) Solve for $\tilde{U}^{s+1}$ in equation (41a), assuming W^s and W^{s+1} are known from the previous iteration

(b) With $\tilde{U}^{s+1}$ now known, solve for $\tilde{W}^{s+1}$ in equation (41b)

(c) Solve for $\tilde{T}^{s+1}$ in (41c), using $\tilde{U}^{s+1}$ and $\tilde{W}^{s+1}$, assuming Θ^{s+1} is known from the previous iteration

(d) With $\tilde{T}^{s+1}$ now known, proceed to solve for $\tilde{\Theta}^{s+1}$ in (41d)

(e) Finally, using $\tilde{U}^{s+1}$, $\tilde{W}^{s+1}$, and $\tilde{T}^{s+1}$, solve for $\tilde{C}^{s+1}$ in (41e)

Beginning with the initial guesses, steps (a) to (e) are repeated, in turn, for $s = 0, 1, 2, \cdots$ to derive approximate solutions to the given model.

3.2. Error, Stability, and Convergence Analysis

3.2.1. Error Bound. Following the approach in Bhrawy [83] and Samuel and Motsa [84], in this subsection, we present an analytical expression for the error norm and an upper bound on the expected error of the approximation, equation (34), to the smooth function $u(x, z, t) \in \Omega \equiv [a, b] \times [c, d] \times [0, T]$. Let

$$\prod = \text{Span}\left\{L_i(x)L_j(z)L_k(t), \forall i = 0, 1, 2, \cdots, N_x ; j = 0, 1, 2, \cdots, N_z ; k = 0, 1, 2, \cdots, N_t\right\}. \tag{42}$$

Given a smooth function $u(x, z, t) \in \Omega \equiv [a, b] \times [c, d] \times [0, T]$. Let $U_N(x, z, t)$, defined in (34), be the best approximation of $u(x, z, t)$ so that $\forall V_N \in \prod$,

$$\|u(x, z, t) - U_N(x, z, t)\|_\infty \le \|u(x, z, t) - V_N(x, z, t)\|_\infty. \tag{43}$$

Then, there exists arbitrary points $\gamma_1, \gamma_1' \in [a, b]$, $\gamma_2, \gamma_2' \in [c, d]$, and $\gamma_3, \gamma_3' \in [0, T]$, so that

$$\begin{aligned} u(x, z, t) - V_N(x, z, t) = {} & \frac{\partial^{N_x+1} u(\gamma_1, z, t)}{\partial x^{N_x+1}(N_x+1)!} \prod_{i=0}^{N_x} (x - x_i) \\ & + \frac{\partial^{N_z+1} u(x, \gamma_2, t)}{\partial z^{N_z+1}(N_z+1)!} \prod_{j=0}^{N_z} (z - z_j) \\ & + \frac{\partial^{N_t+1} u(x, z, \gamma_3)}{\partial t^{N_t+1}(N_t+1)!} \prod_{k=0}^{N_t} (t - t_k) \\ & - \frac{\partial^{N_x+N_z+N_t+3} u(\gamma_1, \gamma_2, \gamma_3)}{\partial x^{N_x+1} \partial z^{N_z+1} \partial t^{N_t+1} (N_t+1)!(N_z+1)!(N_x+1)!} \\ & \times \prod_{i=0}^{N_x} (x - x_i) \times \prod_{j=0}^{N_z} (z - z_j) \times \prod_{k=0}^{N_t} (t - t_k), \end{aligned} \tag{44}$$

where $V_N(x, z, t)$ is the multivariate chebyshev interpolating polynomial of $u(x, z, t)$ at x_i, z_j, and t_k.

Taking the infinite norm of equation (44) yields

$$\begin{aligned} \|u(x, z, t) - V_N(x, z, t)\|_\infty \le {} & \max_{(x,z,t)\in\Omega} \left| \frac{\partial^{N_x+1} u(\gamma_1, z, t)}{\partial x^{N_x+1}} \right| \frac{\left\| \prod_{i=0}^{N_x} (x - x_i) \right\|}{(N_x+1)!} \\ & + \max_{(x,z,t)\in\Omega} \left| \frac{\partial^{N_z+1} u(x, \gamma_2, t)}{\partial z^{N_z+1}} \right| \frac{\left\| \prod_{j=0}^{N_z} (z - z_j) \right\|}{(N_z+1)!} \\ & + \max_{(x,z,t)\in\Omega} \left| \frac{\partial^{N_t+1} u(x, z, \gamma_3)}{\partial t^{N_t+1}} \right| \frac{\left\| \prod_{k=0}^{N_t} (t - t_k) \right\|}{(N_t+1)!} \\ & - \max_{(x,z,t)\in\Omega} \left| \frac{\partial^{N_x+N_z+N_t+3} u\left(\gamma_1', \gamma_2', \gamma_3'\right)}{\partial x^{N_x+1} \partial z^{N_z+1} \partial t^{N_t+1}} \right| \\ & \times \frac{\left\| \prod_{i=0}^{N_x} (x - x_i) \right\| \times \left\| \prod_{j=0}^{N_z} (z - z_j) \right\| \times \left\| \prod_{k=0}^{N_t} (t - t_k) \right\|}{(N_x+1)!(N_z+1)!(N_t+1)!}. \end{aligned} \tag{45}$$

Since $u(x, z, t)$ is a smooth function on Ω; then, its $(N_x + 1)$, $(N_z + 1)$, $(N_t + 1)$, and $(N_x + N_z + N_t + 3)$-th partial derivatives are both continuous and upper-bounded, so that

$$\begin{cases} \max\limits_{(x,z,t)\in\Omega} \left| \dfrac{\partial^{N_x+1} u(\gamma_1, z, t)}{\partial x^{N_x+1}} \right| \le K_1, \\ \max\limits_{(x,z,t)\in\Omega} \left| \dfrac{\partial^{N_z+1} u(x, \gamma_2, t)}{\partial z^{N_z+1}} \right| \le K_2, \\ \max\limits_{(x,z,t)\in\Omega} \left| \dfrac{\partial^{N_t+1} u(x, z, \gamma_3)}{\partial t^{N_t+1}} \right| \le K_3, \\ \max\limits_{(x,z,t)\in\Omega} \left| \dfrac{\partial^{N_x+N_z+N_t+3} u\left(\gamma_1', \gamma_2', \gamma_3'\right)}{\partial x^{N_x+1} \partial z^{N_z+1} \partial t^{N_t+1}} \right| \le K_4, \end{cases} \tag{46}$$

where K_1, K_2, K_3, and K_4 are arbitrary constants in $\mathbb{R}^+$.

Substituting (46) into (45) yields the norm error bound estimate

$$\begin{aligned} \|u(x, z, t) - V_N(x, z, t)\|_\infty \le {} & K_1 \frac{\left\| \prod_{i=0}^{N_x} (x - x_i) \right\|_\infty}{(N_x+1)!} \\ & + K_2 \frac{\left\| \prod_{j=0}^{N_z} (z - z_j) \right\|_\infty}{(N_z+1)!} + K_3 \frac{\left\| \prod_{k=0}^{N_t} (t - t_k) \right\|_\infty}{(N_t+1)!} - K_4 \\ & \times \frac{\left\| \prod_{i=0}^{N_x} (x - x_i) \right\|_\infty \times \left\| \prod_{j=0}^{N_z} (z - z_j) \right\|_\infty \times \left\| \prod_{k=0}^{N_t} (t - t_k) \right\|_\infty}{(N_t+1)!(N_z+1)!(N_x+1)!}, \end{aligned} \tag{47}$$

where $V_N \in \prod^{N_x, N_z, N_t}$.

However, (47) can be further simplified. From the linear relationships defined in (31), we have

$$(x - x_i) = \frac{1}{2}(b - a)(\tilde{x} - \tilde{x}_i), \quad (z - z_j) = \frac{1}{2}(d - c)(\tilde{z} - \tilde{z}_j), \quad \text{and} \quad (t - t_k) = \frac{1}{2}(\tilde{t} - \tilde{t}_k), \tag{48}$$

so that from (47),

$$\begin{aligned} \left\| \prod_{i=0}^{N_x} (x - x_i) \right\|_\infty &= \left\| \prod_{i=0}^{N_x} \frac{(b-a)}{2} (\tilde{x} - \tilde{x}_i) \right\|_\infty \\ &\le \left(\frac{(b-a)}{2} \right)^{N_x} \max_{\tilde{x}, x_i \in [-1,1]} \left| \prod_{i=0}^{N_x} (\tilde{x} - \tilde{x}_i) \right| \\ &\le \frac{(b-a)^{N_x+1}}{2^{N_x+1}} \max_{\tilde{x}, x_i \in [-1,1]} \left| \prod_{i=0}^{N_x} (\tilde{x} - \tilde{x}_i) \right|. \end{aligned} \tag{49}$$

Using equation (36),

$$L_i(\tilde{x}) = \frac{(-1)^{i+1}\left(1 - \tilde{x}^2\right) T'_{N_x(\tilde{x})}}{\bar{\sigma}_i N_x^2 (\tilde{x} - \tilde{x}_i)}, \quad i = 0, 1, 2, \cdots, N_x, \tag{50}$$

so that the $N_x + 1$-th degree Lagrange polynomial is

$$L_{N_x+1}(\tilde{x}) = \frac{(-1)^{N_x+2}\left(1-\tilde{x}^2\right)T'_{N_x(\tilde{x})}}{\bar{\sigma}_i N_x^2(\tilde{x}-\tilde{x}_i)}. \tag{51}$$

Taking the modulus of equation (51) and rearranging the terms yield

$$|(\tilde{x}-\tilde{x}_i)| = \frac{\left|\left(1-\tilde{x}^2\right)T'_{N_x(\tilde{x})}\right|}{\left|N_x^2 L_{N_x+1}(\tilde{x})\right|}. \tag{52}$$

Since the Chebyshev interpolating polynomial, equation (33) is the solution to the Chebyshev differential equation [85]

$$\left(1-x^2\right)\frac{d^2y}{dx^2} - x\frac{dy}{dx} + n^2 y = 0, \tag{53}$$

for nonnegative integers n, $n \in \mathbb{Z}_0$ and $|x| < 1$, it follows that

$$\left(1-x^2\right)T'_{N_x(x)} = -xT_{N_x}(x) - n^2. \tag{54}$$

Using equation (54) and applying the triangular inequality, equation (52) can then be expressed as

$$|(\tilde{x}-\tilde{x}_i)| \le \frac{\left|-\tilde{x}T_{N_x}(\tilde{x})\right| + \left|-n^2\right|}{\left|N_x^2 L_{N_x+1}(\tilde{x})\right|}. \tag{55}$$

Employing the inequality relation stated in [84] and noting that $|T_{N_x}(\tilde{x})| \le 1, \forall x_i \in [-1, 1]$, then

$$\left|\left(1-\tilde{x}^2\right)T'_{N_x}(\tilde{x})\right| = \left|-\tilde{x}T_{N_x}(\tilde{x})\right| + \left|-n^2\right| \le 2N_x, \tag{56}$$

so that (55) becomes

$$|(\tilde{x}-\tilde{x}_i)| \le \frac{2}{N_x}. \tag{57}$$

Therefore, from (57), $\max_{\tilde{x},x_i\in[-1,1]} |\prod_{i=0}^{N_x}(\tilde{x}-\tilde{x}_i)| \le (2N_x+2)/N_x$. It then also follows from (49) that

$$\begin{aligned}\left\|\prod_{i=0}^{N_x}(x-x_i)\right\|_\infty &\le \frac{(b-a)^{N_x+1}}{2^{N_x+1}} \max_{\tilde{x},x_i\in[-1,1]}\left|\prod_{i=0}^{N_x}(\tilde{x}-\tilde{x}_i)\right| \\ &\le \frac{(2N_x+2)(b-a)^{N_x+1}}{N_x 2^{N_x+1}}.\end{aligned} \tag{58}$$

In a similar manner,

$$\begin{aligned}\left\|\prod_{j=0}^{N_z}(z-z_j)\right\|_\infty &\le \frac{(d-c)^{N_z+1}}{2^{N_z+1}} \max_{\tilde{z},z_j\in[-1,1]}\left|\prod_{j=0}^{N_z}(\tilde{z}-\tilde{z}_i)\right| \\ &\le \frac{(2N_z+2)(d-c)^{N_z+1}}{N_z 2^{N_z+1}},\end{aligned} \tag{59}$$

$$\left\|\prod_{k=0}^{N_t}(t-t_k)\right\|_\infty \le \frac{1}{2^{N_t+1}} \max_{\tilde{t},t_k\in[-1,1]}\left|\prod_{k=0}^{N_t}\left(\tilde{t}-\tilde{t}_k\right)\right|. \tag{60}$$

Substituting (58), (59), and (60) into (47) yields

$$\begin{aligned}\|u(x,z,t) - V_N(x,z,t)\|_\infty &\le K_1\frac{(2N_x+2)(b-a)^{N_x+1}}{N_x 2^{N_x+1}(N_x+1)!} \\ &+ K_2\frac{(2N_z+2)(d-c)^{N_z+1}}{N_z 2^{N_z+1}(N_z+1)!} + K_3\frac{(2N_t+2)}{N_t 2^{N_t+1}(N_t+1)!} - K_4 \\ &\times \frac{(2N_x+2)(b-a)^{N_x+1}\times(2N_z+2)(d-c)^{N_z+1}\times(2N_t+2)}{N_x N_z N_t 2^{N_x+N_z+N_t+3}(N_t+1)!(N_z+1)!(N_x+1)!}.\end{aligned} \tag{61}$$

Hence, by combining (61) and (43), an upper bound of the error for the approximate solutions is obtained. Since the model, equations (10)–(13) and (19), does not have the exact solution, it is inferred that the convergence of the proposed method depends basically on the above error bound.

3.2.2. Stability. According to Noborio et al. [30], the display of dispersions or oscillatory errors in the numerical solutions is completely unavoidable regardless of whether one uses FD or FE methods to simulate transport due to the characteristics of the solute transport equation. Hence, to ensure a generally stable MV-SLQLM, two complementary measures are employed on the basis of solute transport equation, equation (13). First, in reference [86], we investigated the existence and uniqueness of the classical solution to equation (13) using the proposed "VF-EM" technique. Defining an error $\tilde{e} \coloneqq c(t) - \tilde{c}(t)$ and making inference of Ilati and Dehghan [82], the result (see equation 3.10 in [86]) means $\tilde{e}$ is strongly stable. Moreover, the well-posed analysis of equation (13) in time integral also demonstrates that the numerical technique is stable in L^2-norm. Second, we examine numerically the stability of a discretized scheme for convection-diffusion terms in equation (13). Among the existing numerical methods for analyzing scheme's stability on the basis of convection-diffusion terms, Yu et al. [87] observed that majority are usually based on five assumptions, i.e., one-dimensional, linear, first kind boundary condition, free source term, and uniform grid system.

However, from [87], any deviation from the aforementioned five assumptions may attribute to enhanced convective stability. In this study, except for the linear nature, equation (13) is of (2 + 1) dimensions, together with a non-free source term, and boundary conditions of first and second types. It is worth also mentioning that the convective terms of equations (12) and (13) use flow velocity functions derived from the pair of highly nonlinear momentum equations, equations (10) and (11). Moreover, the MV-SLQLM is built on Lagrange interpolation bases that do not depend on the order of nodes (nonuniform) and are optimally stable [88, 89]. In spite of the fact that these properties naturally contribute to a more stable numerical scheme, we further check the stability of the convective-diffusion solution profiles following the study of Abdullah [90]. Using a one-dimension steady convective-diffusion equation, Abdullah

[90] described a linear relationship between grid size and local Pe number;

$$N_{\min} = \begin{cases} \mathrm{mPe} + b, & 3.125 < \mathrm{Pe} \leq 100, \\ 3, & 0 \leq \mathrm{Pe} \leq 3.125, \end{cases} \tag{62}$$

where $N_{\min}$ is the minimum grid size, sufficient for the flow profile to behave physically correctly; Pe is the grid or local Peclet number; and m and b are the slope and intercept constants, respectively. Since we have a low Pe, $0 \leq \mathrm{Pe} \leq 100$, advection-diffusion-reaction equation (13), we investigate the effect of varying Pe on the solute concentration profiles at the minimum grid number, $N_{\min}$.

3.2.3. Convergence. Making inference of (61) and (43), convergence to the expected solution is affirmed by considering the L^{∞}-norm of the difference between successive iterations, using the residual error analysis

$$\left.\begin{aligned} E_{\tilde{U}} &= \max_{0\leq i\leq N_t} \left\| \tilde{U}_{s+1,i} - \tilde{U}_{s,i} \right\|_{\infty}, \\ E_{\tilde{W}} &= \max_{0\leq i\leq N_t} \left\| \tilde{W}_{s+1,i} - \tilde{W}_{s,i} \right\|_{\infty}, \\ E_{\tilde{T}} &= \max_{0\leq i\leq N_t} \left\| \tilde{T}_{s+1,i} - \tilde{T}_{s,i} \right\|_{\infty}, \\ E_{\tilde{\Theta}} &= \max_{0\leq i\leq N_t} \left\| \tilde{\Theta}_{s+1,i} - \tilde{\Theta}_{s,i} \right\|_{\infty}, \\ E_{\tilde{C}} &= \max_{0\leq i\leq N_t} \left\| \tilde{C}_{s+1,i} - \tilde{C}_{s,i} \right\|_{\infty}. \end{aligned}\right\}, \tag{63}$$

defined for the difference between values of successive iterations.

3.3. Numerical Application. Now, we apply the above described procedure, the MV-SLQLM, to the model under consideration, equations (10)–(13) and (19), together with (20a), (20b), (20c), (20d), (20e), and (20f). Beginning with the nonlinear Darcy-Brinkman-Forchheimer equation (equation (10)) in the $x-$direction

$$\frac{\partial u}{\partial t} + \phi u u_x + \phi w u_z = a_1 (u_{xx} + u_{zz}) - a_2 u - a_3 u^2, \tag{64}$$

where $a_1 = 1/\mathrm{Re}$, $a_2 = 1/\mathrm{Re} \cdot \Lambda$, and $a_3 = F^*/\mathrm{Re}$, we employ the QLM to look for the linear expression

$$\begin{aligned} &\alpha_{2,s}(x,z,t) u_s^{''} + 1 + \alpha_{1,s}(x,z,t) u_s' + 1 + \alpha_{0,s}(x,z,t) u_{s+1} \\ &\quad - u_t^{s+1} = R_s(x,z,t), \end{aligned} \tag{65}$$

where

$$R_s(x,z,t) = \sum_{m=0}^{2} \alpha_{m,s}(x,z,t) u_s^m - \mathscr{F}\left(u_s, u_s', u_s^{''}\right), \tag{66a}$$

$$\mathscr{F}\left(u_s, u_s', u_s^{''}\right) = a_1 (u_{xx}^s + u_{zz}^s) - \phi u u_x - \phi w u_z - a_2 u^s - a_3 (u^s)^2, \tag{66b}$$

$$\alpha_{m,s}(x,z,t) = \frac{\partial \mathscr{F}\left(u_s, u_s', u_s^{''}\right)}{\partial u_s^m}, \quad m = 0, 1, 2. \tag{66c}$$

Using equations (66b) and (66c), we have

$$\begin{aligned} \alpha_{0,s}(x,z,t) &= -\phi u_x^s - a_2 - 2a_3 u^s \,;\, \alpha_{1,s}(x,z,t) \\ &= -\phi u^s - \phi w^s \,;\, \alpha_{2,s}(x,z,t) = a_1, \end{aligned} \tag{67}$$

so that

$$R_s(x,z,t) = -(\phi u_x^s u^s + \phi w^s u_z^s) + \phi w^{s+1} u_z^s - a_3 (u^s)^2. \tag{68}$$

Hence, equation (65) becomes

$$\begin{aligned} &a_1 \left(u_{xx}^{s+1} + u_{zz}^{s+1}\right) - \phi u^s u_x^{s+1} - \phi w^s u_z^{s+1} - (\phi u_x^s + a_2 + 2a_3 u^s) u^{s+1} \\ &\quad - u_t^{s+1} - \phi u_z^s w^{s+1} = -\phi (u_x^s u^s + w^s u_z^s) - a_3 (u^s)^2. \end{aligned} \tag{69}$$

Applying the Chebyshev spectral collocation method to equation (69) yields

$$\begin{aligned} &\left[a_1 \left(\vec{I}_{N_t+1} \otimes \vec{I}_{N_z+1} \otimes \frac{1}{h_x^2} \vec{D}_x^2 + \vec{I}_{N_t+1} \otimes \frac{1}{h_z^2} \vec{D}_z^2 \otimes \vec{I}_{N_x+1} \right) \right. \\ &\quad - \phi \,\mathrm{diag}\,(U^s) \left(\vec{I}_{N_t+1} \otimes \vec{I}_{N_z+1} \otimes \frac{1}{h_x} \vec{D}_x \right) - \phi \,\mathrm{diag}\,(W^s) \\ &\quad \cdot \left(\vec{I}_{N_t+1} \otimes \frac{1}{h_z} \vec{D}_z \otimes \vec{I}_{N_x+1} \right) - \mathrm{diag}\,(\phi U_x^s + a_2 + 2a_3 U^s) \\ &\quad \left. - \left(\frac{1}{h_t} \vec{D}_t \otimes \vec{I}_{N_z+1} \otimes \vec{I}_{N_x+1} \right) \right] U^{s+1} \\ &\quad - \phi \,\mathrm{diag}\,(U_z^s) W^{s+1} = -\phi (U_x^s U^s + U_z^s W^s) - (a_3 U^s) U^s, \end{aligned} \tag{70}$$

where $h_x = x_l - x_0/2$, $h_z = z_l - z_0/2$, and $h_t = T/2$; and $\vec{I}_{N_t+1}$, $\vec{I}_{N_x+1}$, and $\vec{I}_{N_z+1}$ are, respectively, identity matrices of sizes $(N_t+1) \times (N_t+1)$, $(N_x+1) \times (N_x+1)$, and $(N_z+1) \times (N_z+1)$.

Since U in equation (70) is known at the boundaries of the domain, rewriting equation (70) for the interior points

of the domain, yields the new expression

$$\begin{aligned}
&\left[a_1\left(\vec{I}_{N_t}\otimes\vec{I}_{N_z-1}\otimes\frac{1}{h_x^2}\left[\vec{D}_x^2\right]_{2:N_x,:}+\vec{I}_{N_t}\otimes\frac{1}{h_z^2}\left[\vec{D}_z^2\right]_{2:N_z,:}\otimes\vec{I}_{N_x-1}\right)\right.\\
&\quad-\operatorname{diag}\left(\phi U_x^s+a_2+2a_3U^s\right)-\phi\operatorname{diag}\left(U^s\right)\\
&\quad\cdot\left(\vec{I}_{N_t}\otimes\vec{I}_{N_z-1}\otimes\frac{1}{h_x}\left[\vec{D}_x\right]_{2:N_x,:}\right)\\
&\quad-\phi\operatorname{diag}\left(W^s\right)\left(\vec{I}_{N_t}\otimes\frac{1}{h_z}\left[\vec{D}_z\right]_{2:N_z,:}\otimes\vec{I}_{N_x-1}\right)\\
&\quad\left.-\left(\frac{1}{h_t}\left[\vec{D}_t\right]_{1:N_t,:}\otimes\vec{I}_{N_z-1}\otimes\vec{I}_{N_x-1}\right)\right]\tilde{U}^{s+1}\\
&\quad-\phi\operatorname{diag}\left(U_z^s\right)W^{s+1}=-\phi\left(U_x^sU^s+U_z^sW^s\right)\\
&\quad-\left(a_3\tilde{U}^s\right)\tilde{U}^s-\left(\psi_{ijk}^1+\tilde{\psi}_{ijk}^1\right)-\left(\sigma_{ijk}^1+\tilde{\sigma}_{ijk}^1\right)+\delta_{ijk}^1,
\end{aligned}\tag{71}$$

where $\tilde{U}=U_{2:N_x,2:N_z,1:N_t}$, and

$$\begin{aligned}
\psi^1=&\,a_1\left(\left[\vec{D}_x^2\right]_{2:N_x,1}\otimes U_{1,2:N_z,1:N_t}\right)\\
&-U^s\left(\left[\vec{D}_x\right]_{2:N_x,1}\otimes U_{1,2:N_z,1:N_t}\right),
\end{aligned}\tag{72a}$$

$$\begin{aligned}
\tilde{\psi}_{ijk}^1=&\,a_1\left(\left[\vec{D}_x^2\right]_{2:N_x,N_x+1}\otimes U_{N_x+1,2:N_z,1:N_t}\right)\\
&-U^s\left(\left[\vec{D}_x\right]_{2:N_x,N_x+1}\otimes U_{N_x+1,2:N_z,1:N_t}\right),
\end{aligned}\tag{72b}$$

$$\begin{aligned}
\sigma_{ijk}^1=&\,a_1\left(\left[\vec{D}_z^2\right]_{2:N_z,1}\otimes U_{2:N_x,1,1:N_t}\right)\\
&-W^s\left(\left[\vec{D}_z\right]_{2:N_z,1}\otimes U_{2:N_x,1,1:N_t}\right),
\end{aligned}\tag{72c}$$

$$\begin{aligned}
\tilde{\sigma}_{ijk}^1=&\,a_1\left(\left[\vec{D}_z^2\right]_{2:N_z,N_z+1}\otimes U_{2:N_x,N_z+1,1:N_t}\right)\\
&-W^s\left(\left[\vec{D}_z\right]_{2:N_z,1}\otimes U_{2:N_x,1,1:N_t}\right),
\end{aligned}\tag{72d}$$

$$\delta_{ijk}^1=-\left(\left[\vec{D}_t\right]_{1:N_t,N_t+1}\otimes U_{2:N_x,2:N_z,N_t+1}\right).\tag{72e}$$

Thus, at step (a) of the LLM, we need to solve for $\tilde{U}^{s+1}$ in the matrix equation (equation (71)) defined as

$$\vec{A}_1\tilde{U}^{s+1}=\vec{B}_1+\vec{K}_1,\tag{73}$$

where

$$\begin{aligned}
\vec{A}_1=&\left[a_1\left(\vec{I}_{N_t}\otimes\vec{I}_{N_z-1}\otimes\frac{1}{h_x^2}\left[\vec{D}_x^2\right]_{2:N_x,:}+\vec{I}_{N_t}\otimes\frac{1}{h_z^2}\left[\vec{D}_z^2\right]_{2:N_z,:}\otimes\vec{I}_{N_x-1}\right)\right.\\
&-\operatorname{diag}\left(\phi U_x^s+a_2+2a_3U^s\right)-\phi\operatorname{diag}\left(U^s\right)\\
&\cdot\left(\vec{I}_{N_t}\otimes\vec{I}_{N_z-1}\otimes\frac{1}{h_x}\left[\vec{D}_x\right]_{2:N_x,:}\right)-\phi\operatorname{diag}\left(W^s\right)\\
&\cdot\left(\vec{I}_{N_t}\otimes\frac{1}{h_z}\left[\vec{D}_z\right]_{2:N_z,:}\otimes\vec{I}_{N_x-1}\right)\\
&\left.-\left(\frac{1}{h_t}\left[\vec{D}_t\right]_{1:N_t,:}\otimes\vec{I}_{N_z-1}\otimes\vec{I}_{N_x-1}\right)\right],
\end{aligned}\tag{74}$$

and

$$\vec{B}_1=-\phi\left(U_x^sU^s+U_z^sW^s\right)-\left(a_3\tilde{U}^s\right)\tilde{U}^s+\phi\operatorname{diag}\left(U_z^s\right)W^{s+1},\tag{75a}$$

$$\vec{K}_1=-\left(\psi_{ijk}^1+\tilde{\psi}_{ijk}^1\right)-\left(\sigma_{ijk}^1+\tilde{\sigma}_{ijk}^1\right)+\delta_{ijk}^1.\tag{75b}$$

In a similar manner, the Darcy-Brinkman-Forchheimer equation (equation (11)) in z – direction is expressed as

$$\frac{\partial w}{\partial t}=-b_0P_z-\phi uw_x-\phi ww_z+b_1\left(w_{xx}+w_{zz}\right)-b_2w-b_3w^2+b_4,\tag{76}$$

where $b_0=1/\phi$, $b_1=1/\mathrm{Re}$, $b_2=1/\mathrm{Re}\cdot\Lambda$, $b_3=F^*/\mathrm{Re}$, and $b_4=1/\phi(Gr^T+Gr^C/\mathrm{Re}^2)$.

Applying the QLM, we obtain

$$\begin{aligned}
&b_1\left(w_{xx}^{s+1}+w_{zz}^{s+1}\right)-\phi u^sw_x^{s+1}-\phi w^sw_z^{s+1}\\
&\quad-\left(\phi w_z^s+b_2+2b_3w^s\right)w^{s+1}-b_0P_z^{s+1}-w_t^{s+1}\\
&\quad-\phi w_x^su^{s+1}=-\phi\left(w_xu^s+w_z^sw^s\right)-\left(b_3w^s\right)w^s-b_4.
\end{aligned}\tag{77}$$

Then, by applying the Chebyshev spectral collocation method to equation (77), we get

$$\begin{aligned}
&\left[b_1\left(\vec{I}_{N_t+1}\otimes\vec{I}_{N_z+1}\otimes\frac{1}{h_x^2}\vec{D}_x^2+\vec{I}_{N_t+1}\otimes\frac{1}{h_z^2}\vec{D}_z^2\otimes\vec{I}_{N_x+1}\right)\right.\\
&\quad-\phi\operatorname{diag}\left(U^s\right)\left(\vec{I}_{N_t+1}\otimes\vec{I}_{N_z+1}\otimes\frac{1}{h_x}\vec{D}_x\right)\\
&\quad-\phi\operatorname{diag}\left(W^s\right)\left(\vec{I}_{N_t+1}\otimes\frac{1}{h_z}\vec{D}_z\otimes\vec{I}_{N_x+1}\right)\\
&\quad-\operatorname{diag}\left(\phi W_z^s+b_2+2b_3W^s\right)\\
&\quad\left.-\left(\frac{1}{h_t}\vec{D}_t\otimes\vec{I}_{N_z+1}\otimes\vec{I}_{N_x+1}\right)\right]W^{s+1}-b_0P_z^{s+1}\\
&\quad-\phi\operatorname{diag}\left(W_x^s\right)U^{s+1}=-\phi\left(W_x^sU^s+W_z^sW^s\right)\\
&\quad-\left(b_3W^s\right)W^s-b_4,
\end{aligned}\tag{78}$$

where h_x, h_z, h_t, $\vec{I}_{N_t+1}$, $\vec{I}_{N_x+1}$, and $\vec{I}_{N_z+1}$ are all defined as before.

Considering the known values of W at the initial and boundary conditions, equation (78) can be rearranged as

$$\begin{aligned}
&\left[b_1\left(\vec{I}_{N_t}\otimes\vec{I}_{N_z-1}\otimes\frac{1}{h_x^2}\left[\vec{D}_x^2\right]_{2:N_x,:}+\vec{I}_{N_t}\otimes\frac{1}{h_z^2}\left[\vec{D}_z^2\right]_{2:N_z,:}\otimes\vec{I}_{N_x-1}\right)\right.\\
&\quad-\phi\,\mathrm{diag}\,(U^s)\left(\vec{I}_{N_t}\otimes\vec{I}_{N_z-1}\otimes\frac{1}{h_x}\left[\vec{D}_x\right]_{2:N_x,:}\right)-\phi\,\mathrm{diag}\,(W^s)\\
&\quad\cdot\left(\vec{I}_{N_t}\otimes\frac{1}{h_z}\left[\vec{D}_z\right]_{2:N_z,:}\otimes\vec{I}_{N_x-1}\right)-\mathrm{diag}\,(\phi W_z^s+b_2+2b_3W^s)\\
&\quad\left.-\left(\frac{1}{h_t}\left[\vec{D}_t\right]_{1:N_t,:}\otimes\vec{I}_{N_z-1}\otimes\vec{I}_{N_x-1}\right)\right]\tilde{W}^{s+1}=b_0\tilde{P}_z^{s+1}\\
&\quad+\phi\,\mathrm{diag}\,(W_x^s)\tilde{U}^{s+1}-\phi\left(\tilde{W}_x^s\tilde{U}^s+\tilde{W}_z^s\tilde{W}^s\right)-\left(b_3\tilde{W}^s\right)\tilde{W}^s\\
&\quad-\left(\psi_{ijk}^2+\tilde{\psi}_{ijk}^2\right)-\left(\sigma_{ijk}^2+\tilde{\sigma}_{ijk}^2\right)+\delta_{ijk}^2-b_4,
\end{aligned}\tag{79}$$

where $\tilde{W}=W_{2:N_x,2:N_z,1:N_t}$, and

$$\begin{aligned}
\psi^2=b_1&\left(\left[\vec{D}_x^2\right]_{2:N_x,1}\otimes W_{1,2:N_z,1:N_t}\right)\\
&-U^s\left(\left[\vec{D}_x\right]_{2:N_x,1}\otimes W_{1,2:N_z,1:N_t}\right),
\end{aligned}\tag{80a}$$

$$\begin{aligned}
\tilde{\psi}_{ijk}^2=b_1&\left(\left[\vec{D}_x^2\right]_{2:N_x,N_x+1}\otimes W_{N_x+1,2:N_z,1:N_t}\right)\\
&-U^s\left(\left[\vec{D}_x\right]_{2:N_x,N_x+1}\otimes W_{N_x+1,2:N_z,1:N_t}\right),
\end{aligned}\tag{80b}$$

$$\begin{aligned}
\sigma_{ijk}^2=b_1&\left(\left[\vec{D}_z^2\right]_{2:N_z,N_z+1}\otimes U_{2:N_x,N_z+1,1:N_t}\right)\\
&-W^s\left(\left[\vec{D}_z\right]_{2:N_z,1}\otimes W_{2:N_x,1,1:N_t}\right),
\end{aligned}\tag{80c}$$

$$\begin{aligned}
\tilde{\sigma}_{ijk}^2=b_1&\left(\left[\vec{D}_z^2\right]_{2:N_z,N_z+1}\otimes U_{2:N_x,N_z+1,1:N_t}\right)\\
&-W^s\left(\left[\vec{D}_z\right]_{2:N_z,N_z+1}\otimes W_{2:N_x,N_z+1,1:N_t}\right),
\end{aligned}\tag{80d}$$

$$\delta_{ijk}^2=-\left(\left[\vec{D}_t\right]_{1:N_t,N_t+1}\otimes W_{2:N_x,2:N_z,N_t+1}\right).\tag{80e}$$

Thus, in step (b) of the LLM, we solve for $\tilde{W}^{s+1}$ in the matrix equation

$$\vec{A}_2\tilde{W}^{s+1}=\vec{B}_2+\vec{K}_2,\tag{81}$$

where

$$\begin{aligned}
\vec{A}_2=&\left[b_1\left(\vec{I}_{N_t}\otimes\vec{I}_{N_z-1}\otimes\frac{1}{h_x^2}\left[\vec{D}_x^2\right]_{2:N_x,:}+\vec{I}_{N_t}\otimes\frac{1}{h_z^2}\left[\vec{D}_z^2\right]_{2:N_z,:}\otimes\vec{I}_{N_x-1}\right)\right.\\
&-\phi\,\mathrm{diag}\,(U^s)\left(\vec{I}_{N_t}\otimes\vec{I}_{N_z-1}\otimes\frac{1}{h_x}\left[\vec{D}_x\right]_{2:N_x,:}\right)\\
&-\phi\,\mathrm{diag}\,(W^s)\left(\vec{I}_{N_t}\otimes\frac{1}{h_z}\left[\vec{D}_z\right]_{2:N_z,:}\otimes\vec{I}_{N_x-1}\right)\\
&-\mathrm{diag}\,(\phi W_z^s+b_2+2b_3W^s)\\
&\left.-\left(\frac{1}{h_t}\left[\vec{D}_t\right]_{1:N_t,:}\otimes\vec{I}_{N_z-1}\otimes\vec{I}_{N_x-1}\right)\right],
\end{aligned}\tag{82}$$

and

$$\vec{B}_2=b_0\tilde{P}_z^{s+1}+\phi\,\mathrm{diag}\,(W_x^s)\tilde{U}^{s+1}-\phi\left(\tilde{W}_x^s\tilde{U}^s+\tilde{W}_z^s\tilde{W}^s\right)-\left(b_3\tilde{W}^s\right)\tilde{W}^s,\tag{83a}$$

$$\vec{K}_2=-\left(\psi_{ijk}^2+\tilde{\psi}_{ijk}^2\right)-\left(\sigma_{ijk}^2+\tilde{\sigma}_{ijk}^2\right)+\delta_{ijk}^2-b_4.\tag{83b}$$

The pressure term $\tilde{P}_z^{s+1}$ is iteratively estimated from an initial guess

$$P(x,z)=\frac{x}{4}-\frac{4}{(\pi)^2\sinh 2\pi}\sinh(\pi x)\cos(\pi z),\tag{84}$$

deduced from the analytical solution [91]

$$P(x,z)=\frac{x}{4}-4\sum_{n=1,\mathrm{odd}}^{\infty}\frac{1}{(n\pi)^2\sinh 2n\pi}\sinh(n\pi x)\cos(n\pi z),\tag{85}$$

of the pressure equation $\nabla^2P=0$, assuming an initial state of $P=0$ everywhere and the zero-flux top and bottom boundary conditions.

Next, we express the heat equation as

$$\begin{aligned}
\frac{\partial T}{\partial t}=&\bar{c}_1\left(\frac{\partial^2T}{\partial x^2}+\frac{\partial^2T}{\partial z^2}\right)-\bar{c}_2\left(u\frac{\partial T}{\partial x}+w\frac{\partial T}{\partial z}\right)\\
&+\bar{c}_3\left(\frac{\partial^2\theta}{\partial x^2}+\frac{\partial^2\theta}{\partial z^2}\right)+\bar{c}_4T+\frac{\phi^2Ec}{\mathrm{Re}}\left(\phi\frac{\partial u}{\partial x}\right)^2,
\end{aligned}\tag{86}$$

where $\bar{c}_1=1/\mathrm{Pr\,Re}$, $\bar{c}_2=\varrho_1\phi^2$, $\bar{c}_3=\phi(Ec\varrho_2L_0D_\theta/\mathrm{Re}\,\phi_e)$, $\bar{c}_4=\delta_1/\mathrm{Pr\,Re}$, and $\bar{c}_5=\phi^2Ec/\mathrm{Re}$.

In terms of the QLM, (86) can be expressed as

$$\begin{aligned}
&\bar{c}_1\left(T_{xx}^{s+1}+T_{zz}^{s+1}\right)-\bar{c}_2u^sT_x^{s+1}-\bar{c}_2w^sT_z^{s+1}+\bar{c}_3\left(\theta_{xx}^{s+1}+\theta_{zz}^{s+1}\right)\\
&\quad+\bar{c}_4T^{s+1}-T_t^{s+1}=-\phi^2\bar{c}_5\left(u_x^s\right)^2.
\end{aligned}\tag{87}$$

Applying the Chebyshev spectral collocation method to equation (87), we get

$$\begin{aligned}&\left[\bar{c}_1\left(\vec{I}_{N_{t+1}}\otimes\vec{I}_{N_z+1}\otimes\frac{1}{h_x^2}\vec{D}_x^2+\vec{I}_{N_{t+1}}\otimes\frac{1}{h_z^2}\vec{D}_z^2\otimes\vec{I}_{N_x+1}\right)\right.\\&\quad-\operatorname{diag}(\bar{c}_2U^s)\left(\vec{I}_{N_{t+1}}\otimes\vec{I}_{N_z+1}\otimes\frac{1}{h_x}\vec{D}_x\right)\\&\quad-\operatorname{diag}(\bar{c}_2W^s)\left(\vec{I}_{N_{t+1}}\otimes\frac{1}{h_z}\vec{D}_z\otimes\vec{I}_{N_x+1}\right)+\operatorname{diag}(c_4)\\&\quad\left.-\left(\frac{1}{h_t}\vec{D}_t\otimes\vec{I}_{N_z+1}\otimes\vec{I}_{N_x+1}\right)\right]T^{s+1}\\&\quad+\bar{c}_3\left(\vec{I}_{N_{t+1}}\otimes\vec{I}_{N_z+1}\otimes\frac{1}{h_x^2}\vec{D}_x^2+\vec{I}_{N_z+1}\otimes\frac{1}{h_z^2}\vec{D}_z^2\otimes\vec{I}_{N_x+1}\right)\Theta^{s+1}\\&=-\phi^2\bar{c}_5(U_x^s)^2,\end{aligned}\tag{88}$$

where h_x, h_z, h_t, $\vec{I}_{N_t+1}$, $\vec{I}_{N_x+1}$, and $\vec{I}_{N_z+1}$ are all as previously described.

In a similar manner, with the known values at the boundaries and initial points, we solve

$$\begin{aligned}&\left[\bar{c}_1\left(\vec{I}_{N_t}\otimes\vec{I}_{N_z-1}\otimes\frac{1}{h_x^2}\left[\vec{D}_x^2\right]_{2:N_x,:}+\vec{I}_{N_t}\otimes\frac{1}{h_z^2}\left[\vec{D}_z^2\right]_{2:N_z,:}\otimes\vec{I}_{N_x-1}\right)\right.\\&\quad-\operatorname{diag}(\bar{c}_2U^s)\left(\vec{I}_{N_t}\otimes\vec{I}_{N_z-1}\otimes\frac{1}{h_x}\left[\vec{D}_x\right]_{2:N_x,:}\right)\\&\quad-\operatorname{diag}(\bar{c}_2W^s)\left(\vec{I}_{N_t}\otimes\frac{1}{h_z}\left[\vec{D}_z\right]_{2:N_z,:}\otimes\vec{I}_{N_x-1}\right)\\&\quad\left.+\operatorname{diag}(c_4)-\left(\frac{1}{h_t}\left[\vec{D}_t\right]_{1:N_t,:}\otimes\vec{I}_{N_z-1}\otimes\vec{I}_{N_x-1}\right)\right]\tilde{T}^{s+1}\\&\quad+\bar{c}_3\left(\tilde{\Theta}_{xx}^{s+1}+\tilde{\Theta}_{zz}^{s+1}\right)=-\phi^2\bar{c}_5(U_x^s)^2-\left(\psi_{ijk}^3+\tilde{\psi}_{ijk}^3\right)\\&\quad-\left(\sigma_{ijk}^3+\tilde{\sigma}_{ijk}^3\right)+\delta_{ijk}^3,\end{aligned}\tag{89}$$

where $\tilde{T}=T_{2:N_x,2:N_z,1:N_t}$, $\tilde{U}^s\approx\tilde{U}^{s+1}$, $\tilde{W}^s\approx\tilde{W}^{s+1}$, $\tilde{\Theta}=\Theta_{2:N_x,2:N_z,1:N_t}$, and

$$\begin{aligned}\psi^3=&\bar{c}_1\left(\left[\vec{D}_x^2\right]_{2:N_x,1}\otimes T_{1,2:N_z,1:N_t}\right)\\&-\bar{c}_2\tilde{U}^s\left(\left[\vec{D}_x\right]_{2:N_x,1}\otimes T_{1,2:N_z,1:N_t}\right),\end{aligned}\tag{90a}$$

$$\begin{aligned}\tilde{\psi}_{ijk}^3=&\bar{c}_1\left(\left[\vec{D}_x^2\right]_{2:N_x,N_x+1}\otimes T_{N_x+1,2:N_z,1:N_t}\right)\\&-\bar{c}_2\tilde{U}^s\left(\left[\vec{D}_x\right]_{2:N_x,N_x+1}\otimes T_{N_x+1,2:N_z,1:N_t}\right),\end{aligned}\tag{90b}$$

$$\begin{aligned}\sigma_{ijk}^3=&\bar{c}_1\left(\left[\vec{D}_z^2\right]_{2:N_z,1}\otimes T_{2:N_x,1,1:N_t}\right)\\&-\bar{c}_2\tilde{W}^s\left(\left[\vec{D}_z\right]_{2:N_z,1}\otimes T_{2:N_x,1,1:N_t}\right),\end{aligned}\tag{90c}$$

$$\begin{aligned}\tilde{\sigma}_{ijk}^3=&\bar{c}_1\left(\left[\vec{D}_z^2\right]_{2:N_z,N_z+1}\otimes T_{2:N_z,N_z+1,1:N_t}\right)\\&-\bar{c}_2\tilde{W}^s\left(\left[\vec{D}_z\right]_{2:N_z,N_z+1}\otimes T_{2:N_x,N_z+1,1:N_t}\right),\end{aligned}\tag{90d}$$

$$\delta_{ijk}^3=-\left(\left[\vec{D}_t\right]_{1:N_t,N_t+1}\otimes T_{2:N_x,2:N_z,N_t+1}\right).\tag{90e}$$

Henceforth, at step (c) of the LLM, we solve the matrix equation,

$$\vec{A}_3\tilde{T}^{s+1}=\vec{B}_3+\vec{K}_3,\tag{91}$$

where

$$\begin{aligned}\vec{A}_3=&\left[\bar{c}_1\left(\vec{I}_{N_t}\otimes\vec{I}_{N_z-1}\otimes\frac{1}{h_x^2}\left[\vec{D}_x^2\right]_{2:N_x,:}+\vec{I}_{N_t}\otimes\frac{1}{h_z^2}\left[\vec{D}_z^2\right]_{2:N_z,:}\otimes\vec{I}_{N_x-1}\right)\right.\\&-\operatorname{diag}(\bar{c}_2U^s)\left(\vec{I}_{N_t}\otimes\vec{I}_{N_z-1}\otimes\frac{1}{h_x}\left[\vec{D}_x\right]_{2:N_x,:}\right)\\&-\operatorname{diag}(\bar{c}_2W^s)\left(\vec{I}_{N_t}\otimes\frac{1}{h_z}\left[\vec{D}_z\right]_{2:N_z,:}\otimes\vec{I}_{N_x-1}\right)\\&\left.+\operatorname{diag}(c_4)\left(\frac{1}{h_t}\left[\vec{D}_t\right]_{1:N_t,:}\otimes\vec{I}_{N_z-1}\otimes\vec{I}_{N_x-1}\right)\right],\end{aligned}\tag{92}$$

and,

$$\vec{K}_3=-\left(\psi_{ijk}^3+\tilde{\psi}_{ijk}^3\right)-\left(\sigma_{ijk}^3+\tilde{\sigma}_{ijk}^3\right)+\delta_{ijk}^3,\tag{93a}$$

$$\vec{B}_3=-\bar{c}_3\left(\tilde{\Theta}_{xx}^s+\tilde{\Theta}_{zz}^s\right)-\phi^2\bar{c}_5\left(\tilde{U}_x^s\right)^2.\tag{93b}$$

Since solving the system (91) requires knowledge of $\tilde{\theta}^{s+1}$, we then consider the moisture equation, which is also coupled with temperature T,

$$R_n\frac{\partial\theta}{\partial t}=(\theta_{xx}+\theta_{zz})-\delta_2\theta_z-\bar{b}(T_{xx}+T_{zz}),\tag{94}$$

where $\bar{b}=Le(T_1-T_0)$. Applying the QLM, we need to solve

$$\left(\theta_{xx}^{s+1}+\theta_{zz}^{s+1}\right)-\delta_2\theta_z^{s+1}-\bar{b}(T_{xx}^s+T_{zz}^s)=R_n\theta_t^{s+1}.\tag{95}$$

Then, applying the Chebyshev spectral collocation method to equation (95), we obtain

$$\begin{aligned}&\left[\left(\vec{I}_{N_{t+1}}\otimes\vec{I}_{N_z+1}\otimes\frac{1}{h_x^2}\vec{D}_x^2+\vec{I}_{N_{t+1}}\otimes\frac{1}{h_z^2}\vec{D}_z^2\otimes\vec{I}_{N_x+1}\right)\right.\\&\quad-\operatorname{diag}(\delta_2)\left(\vec{I}_{N_{t+1}}\otimes\frac{1}{h_z}\vec{D}_z\otimes\vec{I}_{N_x+1}\right)\\&\quad\left.-R_n\left(\frac{1}{h_t}\vec{D}_t\otimes\vec{I}_{N_z+1}\otimes\vec{I}_{N_x+1}\right)\right]\Theta^{s+1}\\&\quad-\bar{b}\left(\vec{I}_{N_{t+1}}\otimes\vec{I}_{N_z+1}\otimes\frac{1}{h_x^2}\vec{D}_x^2+\vec{I}_{N_t+1}\otimes\frac{1}{h_z^2}\vec{D}_z^2\otimes\vec{I}_{N_x+1}\right)T^{s+1}=0,\end{aligned}\tag{96}$$

where h_x, h_z, h_t, $\vec{I}_{N_t+1}$, $\vec{I}_{N_x+1}$, and $\vec{I}_{N_z+1}$ are all as previously described.

Taking all the known initial and boundary values of θ^{s+1} and T^{s+1} to the right-hand side of equation (96), we now solve the equation

$$\begin{aligned}&\left[\left(\vec{I}_{N_t}\otimes\vec{I}_{N_z-1}\otimes\frac{1}{h_x^2}\left[\vec{D}_x^2\right]_{2:N_x,:}+\vec{I}_{N_t}\otimes\frac{1}{h_z^2}\left[\vec{D}_z^2\right]_{2:N_z,:}\otimes\vec{I}_{N_x+1}\right)\right.\\&-\operatorname{diag}(\delta_2)\left(\vec{I}_{N_t}\otimes\frac{1}{h_z}\left[\vec{D}_z\right]_{2:N_z,:}\otimes\vec{I}_{N_x-1}\right)\\&\left.-R_n\left(\frac{1}{h_t}\left[\vec{D}_t\right]_{1:N_t,:}\otimes\vec{I}_{N_z-1}\otimes\vec{I}_{N_x-1}\right)\right]\tilde{\Theta}^{s+1}\\&-\bar{b}\left(T_{xx}^{s+1}+T_{zz}^{s+1}\right)=-\left(\psi_{ijk}^4+\tilde{\psi}_{ijk}^4\right)-\left(\sigma_{ijk}^4+\tilde{\sigma}_{ijk}^4\right)+\delta_{ijk}^4,\end{aligned}\tag{97}$$

where

$$\psi^4=\left(\left[\vec{D}_x^2\right]_{2:N_x,1}\otimes\Theta_{1,2:N_z,1:N_t}\right),\tag{98a}$$

$$\tilde{\psi}_{ijk}^4=\left(\left[\vec{D}_x^2\right]_{2:N_x,N_x+1}\otimes\Theta_{N_x+1,2:N_z,1:N_t}\right),\tag{98b}$$

$$\begin{aligned}\sigma_{ijk}^4=&\left(\left[\vec{D}_z^2\right]_{2:N_z,1}\otimes\Theta_{2:N_x,1,1:N_t}\right)\\&-\delta_2\left(\left[\vec{D}_z\right]_{2:N_z,1}\otimes\theta_{2:N_x,1,1:N_t}\right),\end{aligned}\tag{98c}$$

$$\begin{aligned}\tilde{\sigma}_{ijk}^4=&\left(\left[\vec{D}_z^2\right]_{2:N_z,N_z+1}\otimes\Theta_{2:N_z,N_z+1,1:N_t}\right)\\&-\delta_2\left(\left[\vec{D}_z\right]_{2:N_z,N_z+1}\otimes\Theta_{2:N_x,N_z+1,1:N_t}\right),\end{aligned}\tag{98d}$$

$$\delta_{ijk}^4=-\left(\left[\vec{D}_t\right]_{1:N_t,N_t+1}\otimes\theta_{2:N_x,2:N_z,N_t+1}\right),\tag{98e}$$

so that, at step (d) of the LLM, we solve the matrix equation

$$\vec{A}_4\tilde{\Theta}^{s+1}=\vec{B}_4+\vec{K}_4,\tag{99}$$

where

$$\begin{aligned}\vec{A}_4=&\left[\left(\vec{I}_{N_t}\otimes\vec{I}_{N_z-1}\otimes\frac{1}{h_x^2}\left[\vec{D}_x^2\right]_{2:N_x,:}+\vec{I}_{N_t}\otimes\frac{1}{h_z^2}\left[\vec{D}_z^2\right]_{2:N_z,:}\otimes\vec{I}_{N_x-1}\right)\right.\\&-\operatorname{diag}(\delta_2)\left(\vec{I}_{N_t}\otimes\frac{1}{h_z}\left[\vec{D}_z\right]_{2:N_z,:}\otimes\vec{I}_{N_x-1}\right)\\&\left.-\mathrm{R}_n\left(\frac{1}{h_t}\left[\vec{D}_t\right]_{1:N_t,:}\otimes\vec{I}_{N_z-1}\otimes\vec{I}_{N_x-1}\right)\right],\end{aligned}\tag{100}$$

and

$$\vec{B}_4=\bar{b}(T_{xx}^s+T_{zz}^s),\tag{101a}$$

$$\vec{K}_4=-\left(\psi_{ijk}^4+\tilde{\psi}_{ijk}^4\right)-\left(\sigma_{ijk}^4+\tilde{\sigma}_{ijk}^4\right)+\delta_{ijk}^4.\tag{101b}$$

Finally, applying the QLM, the solute equation

$$\begin{aligned}R_m\frac{\partial C}{\partial t}+\bar{e}_1\left(u\frac{\partial C}{\partial x}+w\frac{\partial C}{\partial z}\right)=&\bar{e}_1\left(\frac{\partial^2 C}{\partial x^2}+\frac{\partial^2 C}{\partial z^2}\right)\\&+\bar{\zeta}\left(\frac{\partial^2 T}{\partial x^2}+\frac{\partial^2 T}{\partial z^2}\right)\\&+\mathfrak{Q}_3C+\mathfrak{Q}_4C_a+\mathfrak{Q}_5,\end{aligned}\tag{102}$$

where $\bar{e}_1=\phi^2$ and $\bar{e}_2=\theta_w/\mathrm{Pe}$ become

$$\begin{aligned}&\bar{e}_2\left(C_{xx}^{s+1}+C_{zz}^{s+1}\right)-\bar{e}_1u^sC_x^{s+1}-\bar{e}_1w^sC_z^{s+1}+(\mathfrak{Q}_3+\mathfrak{Q}_4)C^{s+1}\\&-C_t^{s+1}=-\bar{\zeta}(T_{xx}^s+T_{zz}^s)-\mathfrak{Q}_5.\end{aligned}\tag{103}$$

Now, applying the Chebyshev spectral collocation to equation (103), we obtain

$$\begin{aligned}&\left[\bar{e}_2\left(\vec{I}_{N_{t+1}}\otimes\vec{I}_{N_z+1}\otimes\frac{1}{h_x^2}\vec{D}_x^2+\vec{I}_{N_{t+1}}\otimes\frac{1}{h_z^2}\vec{D}_z^2\otimes\vec{I}_{N_x+1}\right)\right.\\&-\operatorname{diag}(\bar{e}_1U^s)\left(\vec{I}_{N_{t+1}}\otimes\vec{I}_{N_z+1}\otimes\frac{1}{h_x}\vec{D}_x\right)\\&-\operatorname{diag}(\bar{e}_1W^s)\left(\vec{I}_{N_{t+1}}\otimes\frac{1}{h_z}\vec{D}_z\otimes\vec{I}_{N_x-1}\right)\\&\left.+\operatorname{diag}(\mathfrak{Q}_3+\mathfrak{Q}_4)-\left(\frac{1}{h_t}\vec{D}_t\otimes\vec{I}_{N_z+1}\otimes\vec{I}_{N_x+1}\right)\right]C^{s+1}\\&=\left[\bar{\zeta}\left(\vec{I}_{N_{t+1}}\otimes\vec{I}_{N_z+1}\otimes\frac{1}{h_x^2}\vec{D}_x^2+\vec{I}_{N_{t+1}}\otimes\frac{1}{h_z^2}\vec{D}_z^2\otimes\vec{I}_{N_x+1}\right)\right]T^s\\&-\operatorname{diag}(\mathfrak{Q}_5),\end{aligned}\tag{104}$$

where h_x, h_z, h_t, $\vec{I}_{N_t+1}$, $\vec{I}_{N_x+1}$, and $\vec{I}_{N_z+1}$ are all as previously

described. Taking out known values of initial and boundary conditions, we obtain

$$\begin{aligned}&\left[\bar{e}_2\left(\vec{I}_{N_t}\otimes\vec{I}_{N_z-1}\otimes\frac{1}{h_x^2}\left[\vec{D}_x^2\right]_{2:N_x,:}+\vec{I}_{N_t}\otimes\frac{1}{h_z^2}\left[\vec{D}_z^2\right]_{2:N_z,:}\otimes\vec{I}_{N_x-1}\right)\right.\\&\quad-\operatorname{diag}\left(\bar{e}_1U^s\right)\left(\vec{I}_{N_t}\otimes\vec{I}_{N_z-1}\otimes\frac{1}{h_x}\left[\vec{D}_x\right]_{2:N_x,:}\right)\\&\quad-\operatorname{diag}\left(\bar{e}_1W^s\right)\left(\vec{I}_{N_t}\otimes\frac{1}{h_z}\left[\vec{D}_z\right]_{2:N_z,:}\otimes\vec{I}_{N_x-1}\right)\\&\quad\left.+\operatorname{diag}\left(\varrho_3+\varrho_4\right)-\left(\frac{1}{h_t}\left[\vec{D}_t\right]_{1:N_t,:}\otimes\vec{I}_{N_z-1}\otimes\vec{I}_{N_x-1}\right)\right]\tilde{C}^{s+1}\\&=-\bar{\zeta}\left(\tilde{T}^s_{xx}+\tilde{T}^s_{zz}\right)-\left(\psi^5_{ijk}+\tilde{\psi}^5_{ijk}\right)\\&\quad-\left(\sigma^5_{ijk}+\tilde{\sigma}^5_{ijk}\right)+\delta^5_{ijk}-\operatorname{diag}\left(\varrho_5\right),\end{aligned}\tag{105}$$

where $\tilde{C}=C_{2:N_x,2:N_z,1:N_t}$, $\tilde{U}^s\approx\tilde{U}^{s+1}$, $\tilde{W}^s\approx\tilde{W}^{s+1}$, and

$$\begin{aligned}\psi^5_{ijk}&=\bar{e}_2\left(\left[\vec{D}_x^2\right]_{2:N_x,1}\otimes C_{1,2:N_z,1:N_t}\right)\\&\quad-\bar{e}_1\tilde{U}^s\left(\left[\vec{D}_x\right]_{2:N_x,1}\otimes C_{1,2:N_z,1:N_t}\right),\end{aligned}\tag{106a}$$

$$\begin{aligned}\tilde{\psi}^5_{ijk}&=\bar{e}_2\left(\left[\vec{D}_x^2\right]_{2:N_x,N_x+1}\otimes C_{N_x+1,2:N_z,1:N_t}\right)\\&\quad-\bar{e}_1\tilde{U}^s\left(\left[\vec{D}_x\right]_{2:N_x,N_x+1}\otimes C_{N_x+1,2:N_z,1:N_t}\right),\end{aligned}\tag{106b}$$

$$\begin{aligned}\sigma^5_{ijk}&=\bar{e}_2\left(\left[\vec{D}_z^2\right]_{2:N_z,1}\otimes C_{2:N_x,1,1:N_t}\right)\\&\quad-\bar{e}_1\tilde{W}^s\left(\left[\vec{D}_z\right]_{2:N_z,1}\otimes C_{2:N_x,1,1:N_t}\right),\end{aligned}\tag{106c}$$

$$\begin{aligned}\tilde{\sigma}^5_{ijk}&=\bar{e}_2\left(\left[\vec{D}_z^2\right]_{2:N_z,N_z+1}\otimes C_{2:N_z,N_z+1,1:N_t}\right)\\&\quad-\bar{e}_1\tilde{W}^s\left(\left[\vec{D}_z\right]_{2:N_z,N_z+1}\otimes C_{2:N_x,N_z+1,1:N_t}\right),\end{aligned}\tag{106d}$$

$$\delta^5_{ijk}=-\left(\left[\vec{D}_t\right]_{1:N_t,N_t+1}\otimes C_{2:N_x,2:N_z,N_t+1}\right).\tag{106e}$$

Thus, at step (e), we solve for $\tilde{C}^{s+1}$ in the matrix equation

$$\vec{A}_5\tilde{C}^{s+1}=\vec{B}_5+\vec{K}_5,\tag{107}$$

where

$$\begin{aligned}\vec{A}_5=&\left[\bar{e}_2\left(\vec{I}_{N_t}\otimes\vec{I}_{N_z-1}\otimes\frac{1}{h_x^2}\left[\vec{D}_x^2\right]_{2:N_x,:}+\vec{I}_{N_t}\otimes\frac{1}{h_z^2}\left[\vec{D}_z^2\right]_{2:N_z,:}\otimes\vec{I}_{N_x-1}\right)\right.\\&-\operatorname{diag}\left(\bar{e}_1U^s\right)\left(\vec{I}_{N_t}\otimes\vec{I}_{N_z-1}\otimes\frac{1}{h_x}\left[\vec{D}_x\right]_{2:N_x,:}\right)\\&-\operatorname{diag}\left(\bar{e}_1W^s\right)\left(\vec{I}_{N_t}\otimes\frac{1}{h_z}\left[\vec{D}_z\right]_{2:N_z,:}\otimes\vec{I}_{N_x-1}\right)\\&\left.+\operatorname{diag}\left(\varrho_3+\varrho_4\right)-\left(\frac{1}{h_t}\left[\vec{D}_t\right]_{1:N_t,:}\otimes\vec{I}_{N_z-1}\otimes\vec{I}_{N_x-1}\right)\right],\end{aligned}\tag{108}$$

and

$$\vec{K}_5=-\left(\psi^5_{ijk}+\tilde{\psi}^5_{ijk}\right)-\left(\sigma^7_{ijk}+\tilde{\sigma}^7_{ijk}\right)+\delta^5_{ijk}-\operatorname{diag}\left(\rho_5\right),\tag{109a}$$

$$\vec{B}_5=-\bar{\zeta}\left(\tilde{T}^s_{xx}+\tilde{T}^s_{zz}\right).\tag{109b}$$

The spectral-collocated field variables at the initial and boundary points are then given by

$$\begin{aligned}\overrightarrow{\tilde{U}}^{s+1}(:,:,1)&=0,\ \tilde{T}^{s+1}(:,:,1)\\&=T_i,\ \tilde{\Theta}^{s+1}(:,:,1)\\&=\theta_0,\ \tilde{C}^{s+1}(:,:,1)=C_i,\end{aligned}\tag{110a}$$

$$\begin{aligned}\tilde{U}^{s+1}(N_x+1,:,:)&=\frac{U_{wm}}{U_0\phi},\ \tilde{W}^{s+1}(1,:,:)\\&=0,\ \tilde{W}^{s+1}(N_x+1,:,:)\\&=0,\ \tilde{U}^{s+1}(1,:,:)\\&=\frac{U_{wm}}{U_0\phi},\end{aligned}\tag{110b}$$

$$\begin{aligned}\tilde{U}^{s+1}(:,N_z+1,:)&=0,\ \tilde{U}^{s+1}(:,1,:)\\&=0,\ \tilde{W}^{s+1}(:,N_z+1,:)\\&=0,\ \tilde{W}^{s+1}(:,1,:)\\&=\frac{V_{wm}}{U_0^2\phi},\end{aligned}\tag{110c}$$

$$\begin{aligned}&\left(\vec{I}_{N_t+1}\otimes\vec{I}_{N_z+1}\otimes\vec{D}^{(1)}_{N_x+1,:,:}\right)\tilde{T}^{s+1}\\&\quad=\frac{q'd}{(T_0-T_i)},\ \left(\vec{I}_{N_t+1}\otimes\vec{I}_{N_z+1}\otimes\vec{D}^{(1)}_{1,:,:}\right)\tilde{T}^{s+1}\\&\quad=\frac{q'd}{(T_0-T_i)},\end{aligned}\tag{110d}$$

Table 1: Dimensionless model numbers and parameter values.

	Symbol	Description	Value range	Reference(s)
Numbers	Re_p	Pores' Reynolds number, laminar Darcy flows	$10^{-2} - 10^{1}$	[40]
	$D'a$	Darcy number	$3.33 \times 10^{-6} - 3.33 \times 10^{-3}$	[92]
	F'	Forchheimer number	e^*	[40]
	Gr^C	Concentration Grashof number	1.12 – 4.2	[93]
	Gr^T	Temperature Grashof number	0.67 – 3.31	[93]
	Pr	Prandtl number	1.0—15	[94]
	Ec	Eckert number	1.8	[74, 95]
	Pe	Peclet number	0.05 – 5.0	[23, 96]
	Da	Damköhler number	1.0 – 11.5	[23]
	Le'	Lewis number	e^*	Eq. (19)
Parameters	ϱ_1	Heat capacity ratio	0.01	[95]
	ϱ_2	Characteristic time	e^*	L/U_0
	δ_1	Heat generation/absorption	2.0	[95]
	ϱ'_3	Apparent Danköhler number	e^*	equation (27)
	ϱ'_4	Weighted Danköhler number	e^*	equation (29)
	ϱ'_5	Apparent chemical sink	e^*	equation (29)
	R_m	Matrix retardation factor	e^*	equation (13)
	δ_2	Apparent diffusion ratio	e^*	equation (19)
	R_n	Moisture retardation factor	e^*	equation (19)

Note: e^* means that the value is empirically estimated. The empirical values are computed at $\theta_r = 0.124\,\mathrm{m^3 m^{-3}}$, $\theta_s = 0.495\,\mathrm{m^3 m^{-3}}$, $C_0 = 0.125\,\mathrm{Mgm^{-3}}$, $C_i = 0.1\,\mathrm{Mgm^{-3}}$, and $C_s = 0.211\,\mathrm{Mgm^{-3}}$.

$$\begin{aligned}\tilde{T}^{s+1}(:,N_z+1,:) &= \frac{-T_i}{(T_0 - T_i)}, \tilde{T}^{s+1}(:,1,:) \\ &= \frac{(T_0 - 2T_i)}{(T_0 - T_i)}, \tilde{C}^{s+1}(:,N_z+1,:) \\ &= 0,\end{aligned} \tag{110e}$$

$$\begin{aligned}&\left(\vec{I}_{N_t+1} \otimes \vec{I}_{N_z+1} \otimes \vec{D}^{(1)}_{N_x+1,:,:}\right)\tilde{C}^{s+1} \\ &= 0, \left(\vec{I}_{N_t+1} \otimes \vec{I}_{N_z+1} \otimes \vec{D}^{(1)}_{1,:,:}\right)\tilde{C}^{s+1} \\ &= 0, \tilde{C}^{s+1}(:,1,:) = 1,\end{aligned} \tag{110f}$$

$$\begin{aligned}&\left(\vec{I}_{N_t+1} \otimes \vec{I}_{N_z+1} \otimes \vec{D}^{(1)}_{N_x+1,:,:}\right)\tilde{\Theta}^{s+1} \\ &= \frac{E_x d}{(\theta_s - \theta_r)}, \left(\vec{I}_{N_t+1} \otimes \vec{I}_{N_z+1} \otimes \vec{D}^{(1)}_{1,:,:}\right)\tilde{\Theta}^{s+1} \\ &= \frac{E_x d}{(\theta_s - \theta_r)},\end{aligned} \tag{110g}$$

$$\tilde{\Theta}^{s+1}(:,N_z+1,:) = 0, \tilde{\Theta}^{s+1}(:,1,:) = \frac{(\theta_0 - \theta_r)}{(\theta_s - \theta_r)}. \tag{110h}$$

Then, starting from initial guesses, we obtain approximate solutions for $u(x,z,t)$, $w(x,z,t)$, $T(x,z,t)$, $\theta(x,z,t)$, and $C(x,z,t)$ by iteratively solving the matrix equations (73), (81), (91), (99), and (107), in turn, for $s = 0, 1, 2, \cdots$. We only confirm convergence to the expected solutions by measuring the norm residual errors of the difference between successive iterations as defined in (64).

4. Numerical Simulations and Discussion

In this section, numerical results of the stability and convergence analyses of the proposed method over the given model are presented and discussed. A convergence test using residual errors is conducted to examine the accuracy of the scheme. To further validate its performance, numerical computations of the various flow profiles of the model are presented to demonstrate applicability of the proposed MV-SLQLM. In computing the numerical results, we use the model parameter values presented in Tables 1 and 2. All computations were performed on an Intel core i7 processor of 8th Generation using MATLAB R2015a.

4.1. Stability and Rate of Convergence. At varying local Pe, changes in the solute concentration profile for the given grid numbers are shown in Figure 2.

From Figure 2, stability of the numerical method is more pronounced when solving equation (13) with local Pe > 2, particularly for the collocation points $N_x = N_z = 20$ and $N_t = 5$ (see Figure 2(b)). The reason is that, unlike in

Table 2: Parameter values for loamy sand soil considered for laminar flow.

Thermodynamic, transport, and soil properties				
Parameter	Description	SI unit	Value (s)	Source
K_h	Soil thermal conductivity	$\mathrm{J}(\mathrm{s}^{-1})^{\circ}\mathrm{C}^{-1}$	$45.318 \times \theta^{*0.6619}$	[39]
ϕ	Porosity	$(-)$	$0 - 1$	[36]
k	Permeability	m^2	$10^{-20} - 10^{-5}$	[40]
K_θ	Hydraulic conductivity	ms^{-1}	$10^{-7} - 10^{-3}$	[41]
ζ_s	Water uptake/sink	day^{-1}	$0.013 - 0.386$	[97] [22]
D_o	Molecular diffusion of NaCl in water	$\mathrm{m}^2\mathrm{s}^{-1}$	$1 \times 10^{-9} - 2 \times 10^{-9}$	[18] [31, 39]
K_s	Saturated hydraulic conductivity	ms^{-1}	$1.23 \times 10^{-7} - 6.67 \times 10^{-6}$	[1] [97] [98]
D_x	Soil thermal diffusivity	$\mathrm{m}^2\mathrm{s}^{-1}$	$5.78 \times 10^{-9} - 4.44 \times 10^{-7}$	[1]
θ_r	Residual moisture content	$(-)$	$0.005 - 0.027$	[31, 39]
θ_s	Saturated moisture content	$(-)$	$0.350 - 0.396$	[31, 39] [97, 98]
θ_w	Medium water content	$(-)$	$0.029 - 0.454$	[30] [99]
F	Forchheimer coefficient	$(-)$	$0.0 - 0.5$	[40]
ρ_b	Average bulk density	Mgm^{-3}	1.470	[31, 39]
L_o	Latent heat of vaporization	Jkg^{-1}	$2.5 \times 10^6 - 2369.2T^*$	[31, 100]
D_T	Moisture diffusivity under temperature gradient	$\mathrm{m}^2(\mathrm{s}^{-1})^{\circ}\mathrm{C}^{-1}$	$3.6 \times 10^{-14.012} \times T^{*6.9146}$	[39]
κ_d	Distribution coefficient	$\mathrm{L}^3\mathrm{Mg}^{-1}$	$0.013 - 0.086$	[22, 101]

Note: *-empirically estimated at $T^* = 25^{\circ}\mathrm{C}$; $\theta^* = \theta_w$.

Figure 2(b), the convection-diffusion-reaction numerical solution is more sensitive to the data perturbations in Figures 2(a), 2(c), and 2(d). Particularly, we notice from Figure 2 that stability deteriorates as the number of spatial collocation points increases (see Figures 2(c) and 2(d)). Further, for successively increased number of spatial collocation points, Figures 3–7 show the infinity error norms at different iteration points for each equation in the model.

Since the present scheme is limited to short temporal domains, the number of collocation points in time was fixed to $N_t = 5$. Nonetheless, overall, the results show that solution errors introduced in one iteration step do not accumulate in the successive iteration points, affirming general stability of the MV-SLQLM, perhaps as attributed to the optimally stable property of Lagrange interpolation basis function also [88, 89]. Moreover, despite using small values of N_x, N_z, and N_t (see Figures 3 and 4), we obtain highly accurate solutions to the model using the present method. However, from the inspection of Figure 6, the $N_x = N_z = 20$ and $N_t = 5$ collocation points are sufficient to give accurate and consistent results. The reason is that, unlike at 20×20 spatial collocation points, jumps and oscillating wiggles appear at the right end of iteration domain in the solute equation for 15×15 (see Figure 5) and 25×25 (see Figure 7) collocation points, respectively. The excellent superexponential convergence of residual errors to almost machine precision level (Figure 6) is an indication that the proposed MV-SLQLM is reliable to model the distribution and interaction of heat and mass transfer in the porous media.

In Table 3, the numerical results based on running/CPU time and condition number of the coefficient matrices, obtained using the proposed method, are compared with those presented by the TV-SCM [84] and MV-SQLM [72] at two subinterval lengths $[0, T]$ in t variable and using the same number of collocation points in the spatial and time domains.

From the inspection of Table 3, we observe that for each method, both the computational time and condition number increase with time, T but with small values recorded for the MV-SLQLM. The present results suggest that employing the LLM to decouple the quasilinearized equations saves more on computational time than solving it as a compact matrix system of quasilinearized equations (see [72, 84]). Furthermore, in agreement with Hidayat et al. [49], Table 3 shows that low computational effort of collocation is indeed guaranteed for schemes with Kronecker delta properties. This is evidenced from a comparison of MV-SLQLM and MV-SQLM in terms of CPU times, which both use Kronecker delta properties, suggesting that the current proposed method (MV-SLQLM) is more efficient than the TV-SCM [84] and MV-SQLM [72] at solving large coupled systems of PDEs.

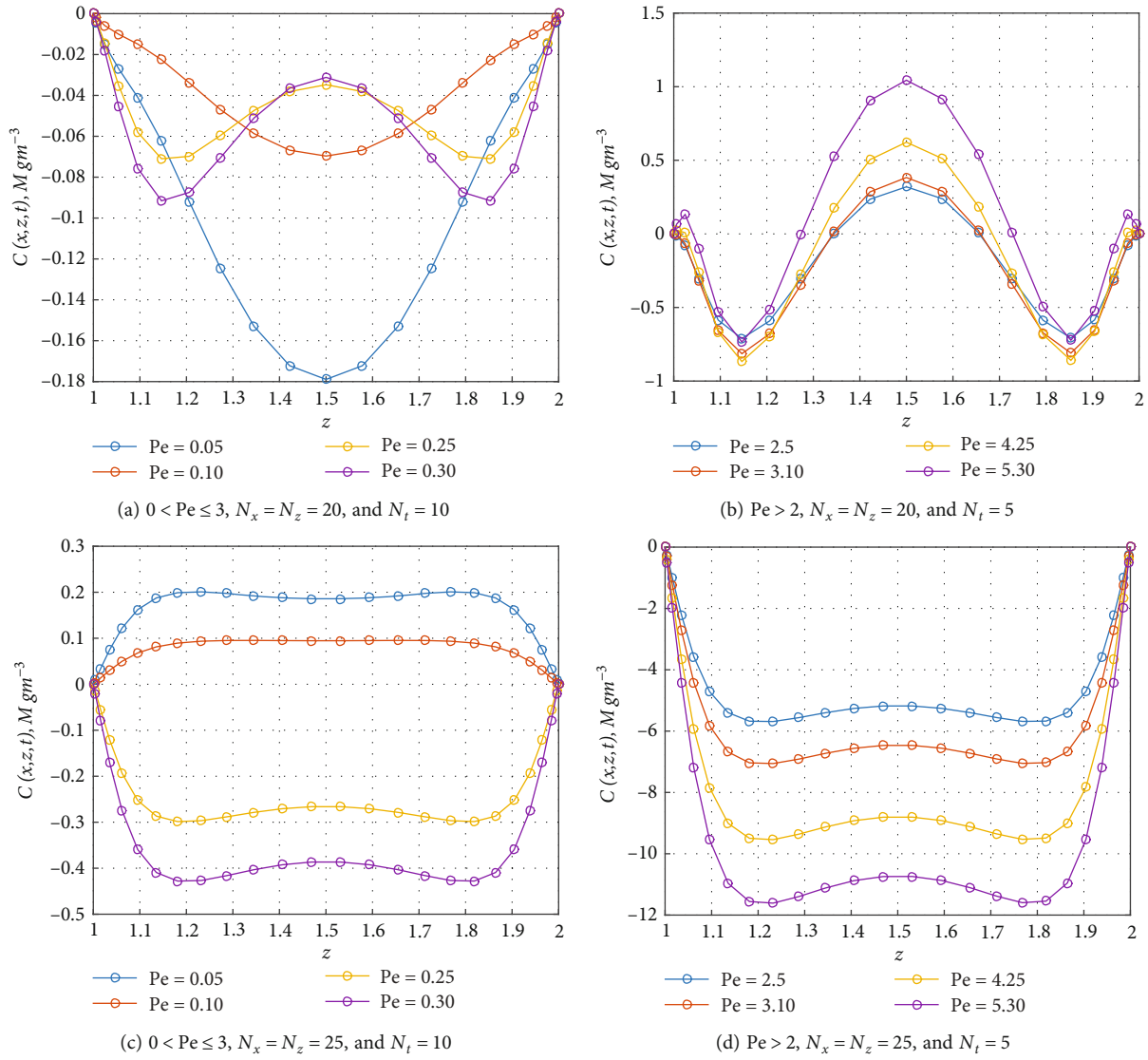

(a) $0 < \text{Pe} \leq 3$, $N_x = N_z = 20$, and $N_t = 10$

(b) $\text{Pe} > 2$, $N_x = N_z = 20$, and $N_t = 5$

(c) $0 < \text{Pe} \leq 3$, $N_x = N_z = 25$, and $N_t = 10$

(d) $\text{Pe} > 2$, $N_x = N_z = 25$, and $N_t = 5$

FIGURE 2: Effect of varying local Pe on the distribution of solute concentration profile at different collocation points.

4.2. Validation. The local linearization method (LLM) described by equations (41a)–(41e) and the subsequent steps (a)–(e) are then used to generate approximate numerical solutions for the system of governing equations (10)–(13). The linearized equations (73), (81), (91), (99), and (107) are then subsequently solved using the MV-SLQLM. The numerical values of pertinent parameters are kept fixed as $\phi = 0.62$, $F = 0.5$, $\Lambda = 1.3$, $Gr^C = 2.02$, $Gr^T = 1.07$, $R_n = 1.0$, $\text{Le} = 0.31$, $\text{Ec} = 1.8$, $\text{Re}_p = 1.05$, $\text{Da} = 2.5$, $\text{Pr} = 0.2$, $\text{Pe} = 0.25$, $\kappa_d = 0.013$, and $\zeta_s = 0.257$, otherwise stated. The numerical simulations are discussed in comparison with published results in the literature. In addition, $N_x = N_z = 20$ and $N_t = 5$ collocation points in the space and time domain, respectively, sufficient to give accurate and consistent results are used.

4.2.1. Velocity Distribution. Figure 8 illustrates the variation of velocity profile against depth z for the vertical preferential flow at changes in ϕ, Re_p, Gr^T, Gr^C, F, and Λ, while the other parameters keep constant and read as described above.

As expected, velocity reduces for greater values of porosity and Forchheimer number due to the increase in viscosity. The effect of varying porosity ϕ and Forchheimer number on velocity profile is shown in Figures 8(a) and 8(e), respectively. As it is found, for higher values of ϕ or Forchheimer number, indeed velocity reduces. Physically, the porous medium characterizes one of the types of external resistance forces that work to resist the movement of the fluid through it, and thus, the velocity of the fluid decreases. Figure 8(f) shows the effect of varying the Darcy number Λ on the velocity distribution W, ms^{-1}. Literature retains that increasing the values of Darcy number changes the rate of fluid-permeability through the porous medium, thereby leading to a reduced velocity distribution. However, through the present study, the velocity distribution of the fluid continually increases with the Darcy number Λ enhancement, consistent with [35]. Perhaps, the reason is that at low values Λ, as caused by a reduction in the medium's permeability k, there is an increase in flow resistance. It is therefore an increase in capillary pressure,

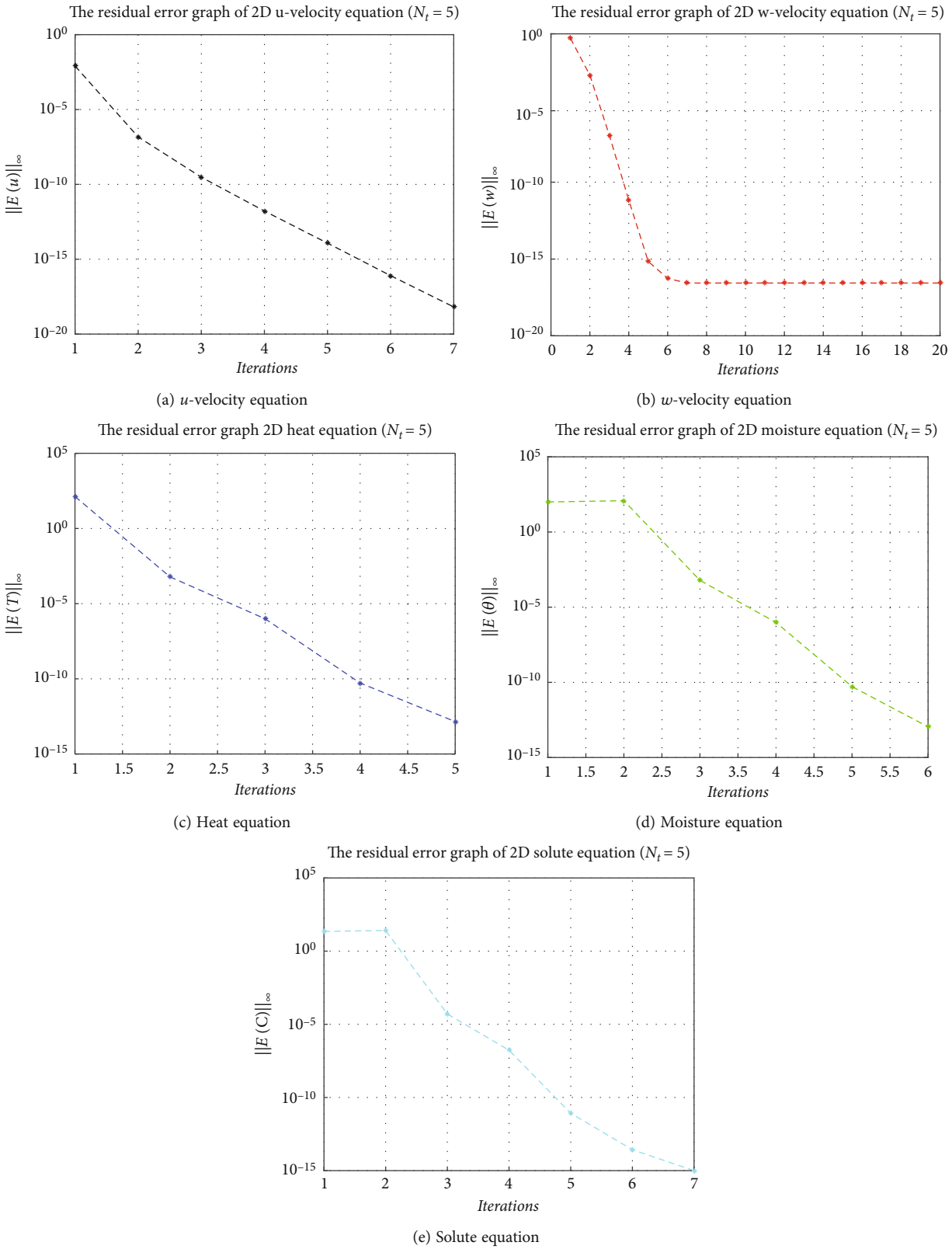

Figure 3: Error norms at different iteration points of the model, for $N_x = N_z = 5$ and $N_t = 5$.

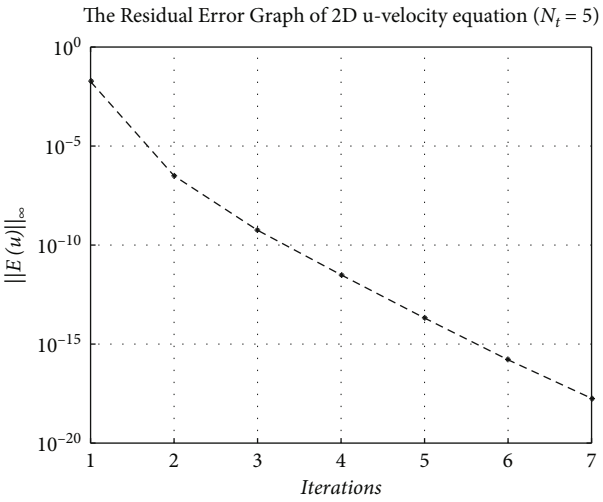

(a) u-velocity equation

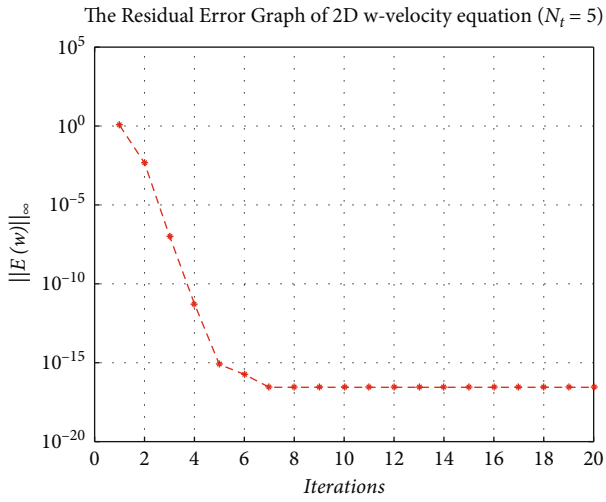

(b) w-velocity equation

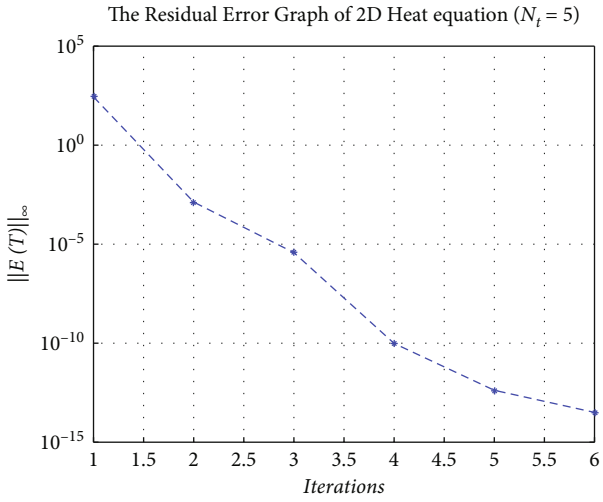

(c) Heat equation

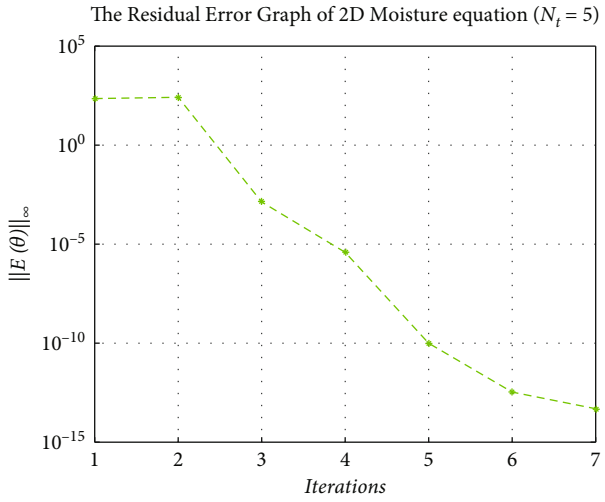

(d) Moisture equation

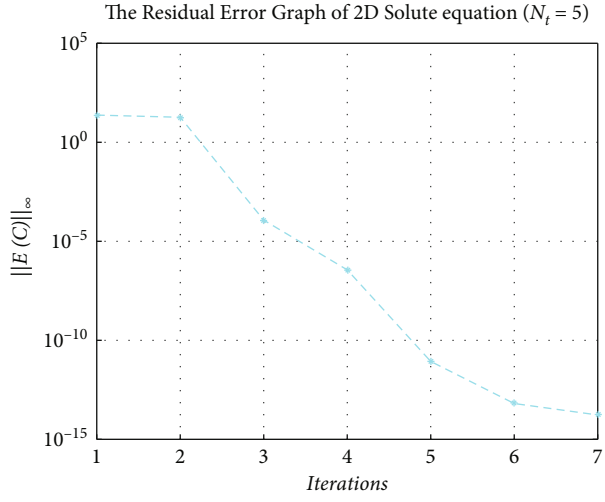

(e) Solute equation

Figure 4: Error norms at different iteration points of the model, for $N_x = N_z = 10$ and $N_t = 5$.

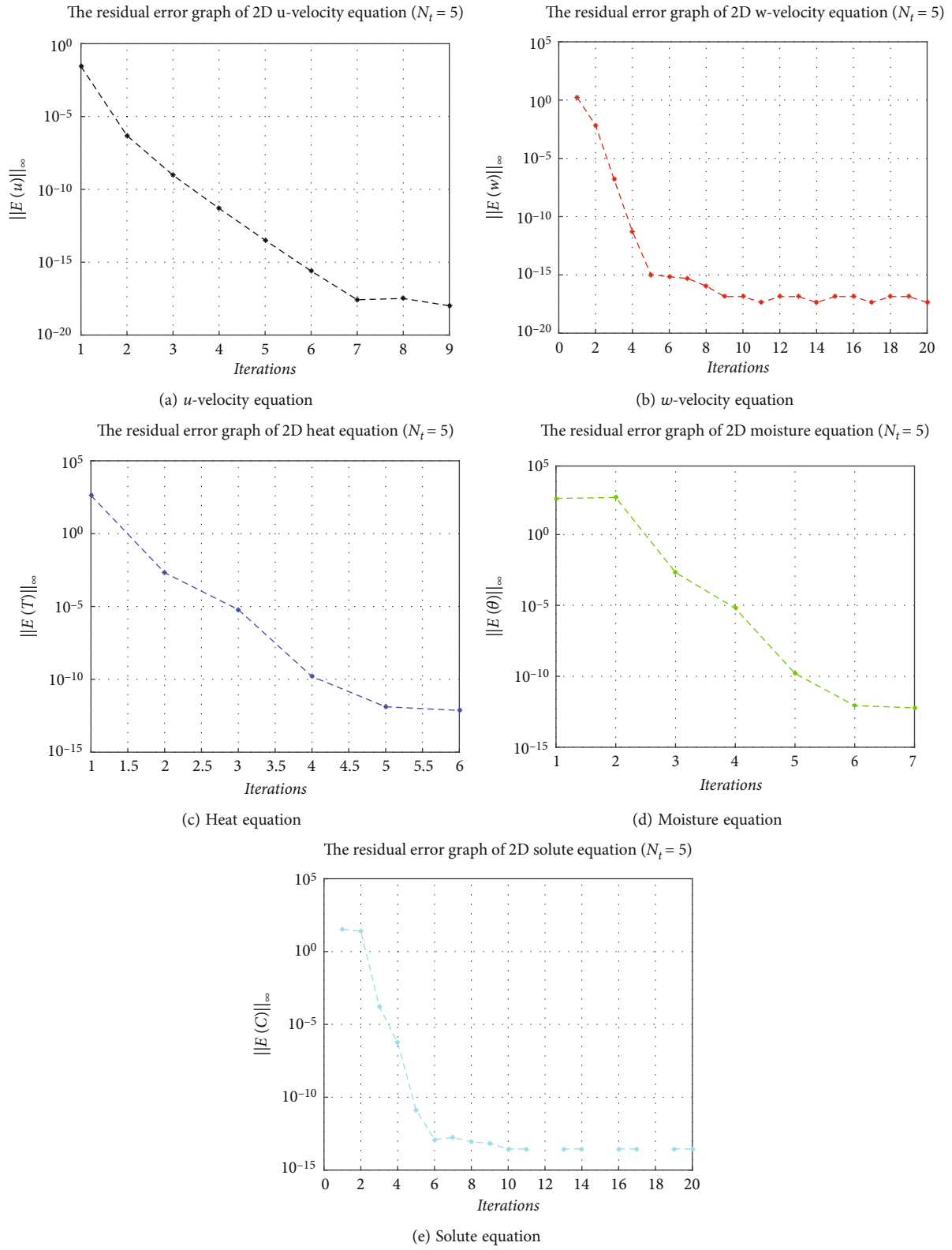

FIGURE 5: Error norms at different iteration points of the model, for $N_x = N_z = 15$ and $N_t = 5$.

due to flow resistance, which causes a reduction in velocity of flow at low Λ numbers. For higher values of Grashof number Gr, however, velocity distribution enhances because of the decrease in viscous forces. In agreement, Figures 8(c) and 8(d) show that the velocity distribution increases with increase in Gr^T and Gr^C.

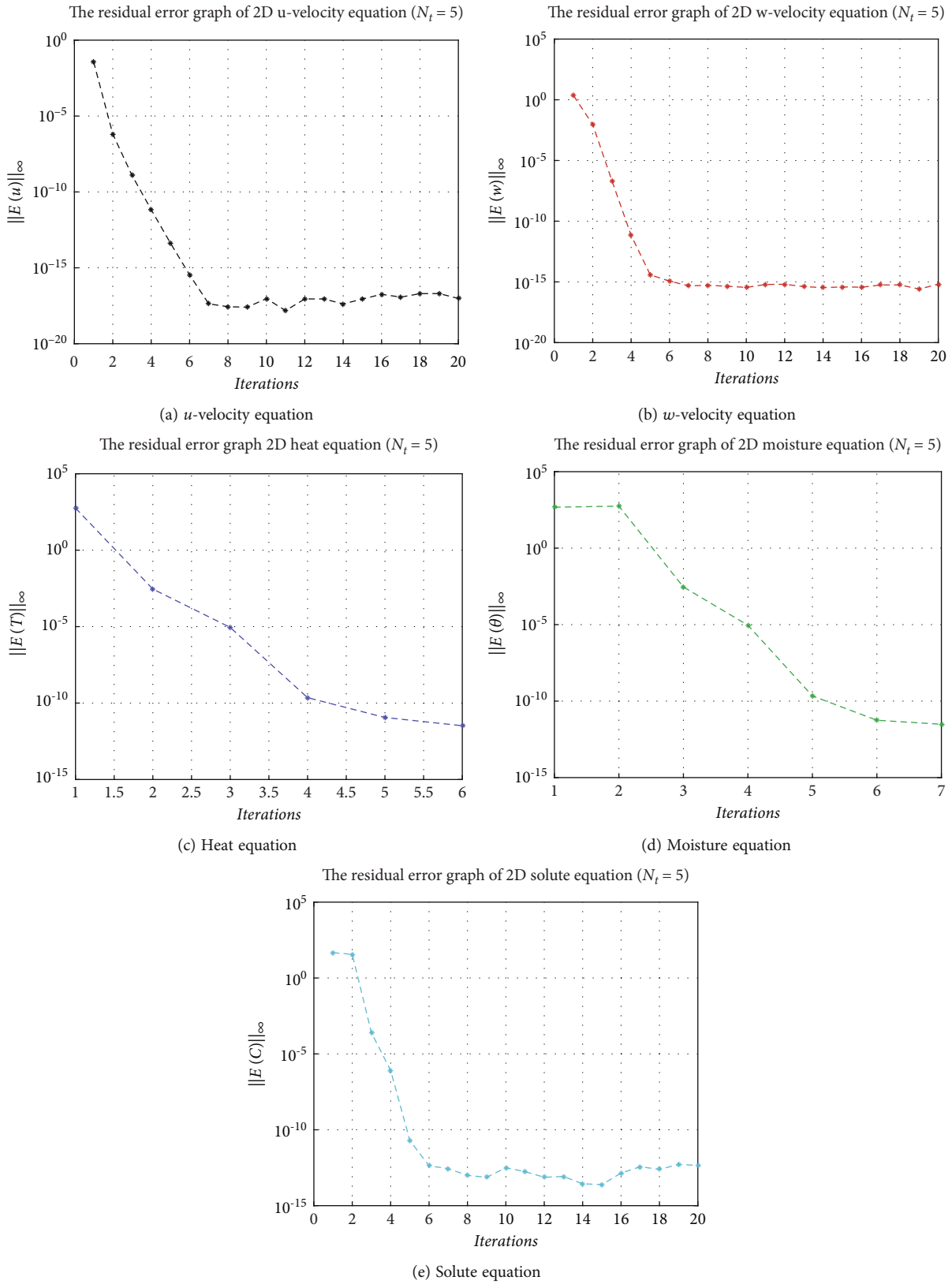

(a) u-velocity equation

(b) w-velocity equation

(c) Heat equation

(d) Moisture equation

(e) Solute equation

Figure 6: Error norms at different iteration points of the model, for $N_x = N_z = 20$ and $N_t = 5$.

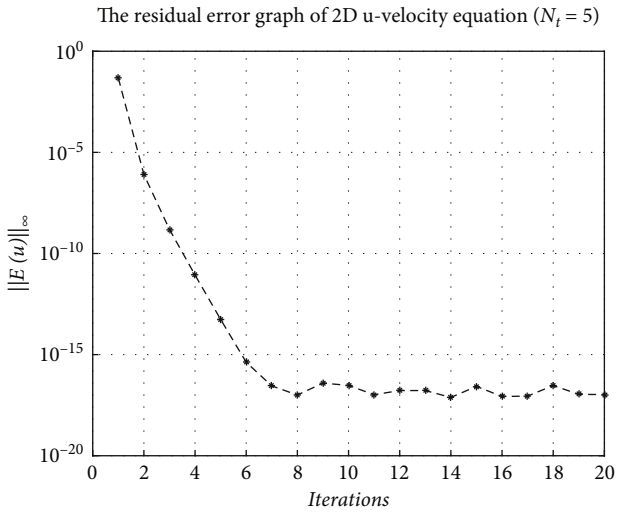

(a) u-velocity equation

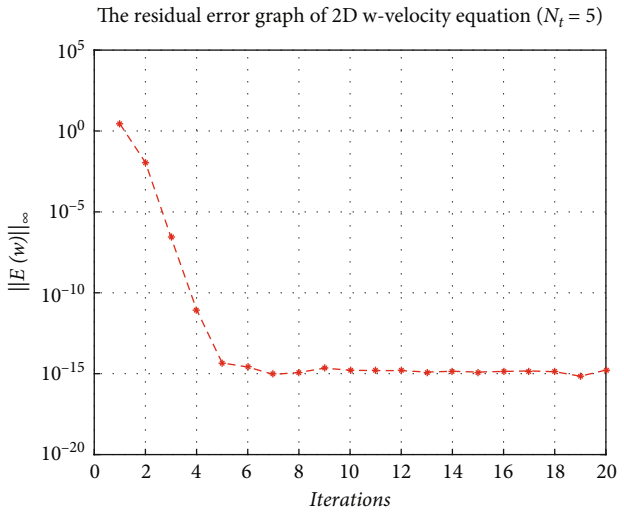

(b) w-velocity equation

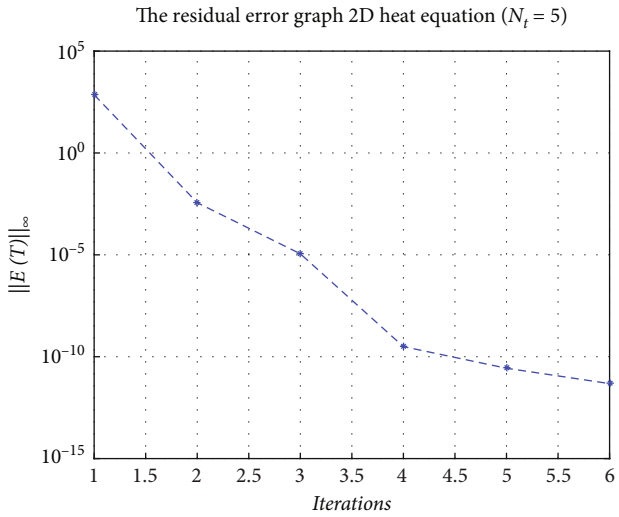

(c) Heat equation

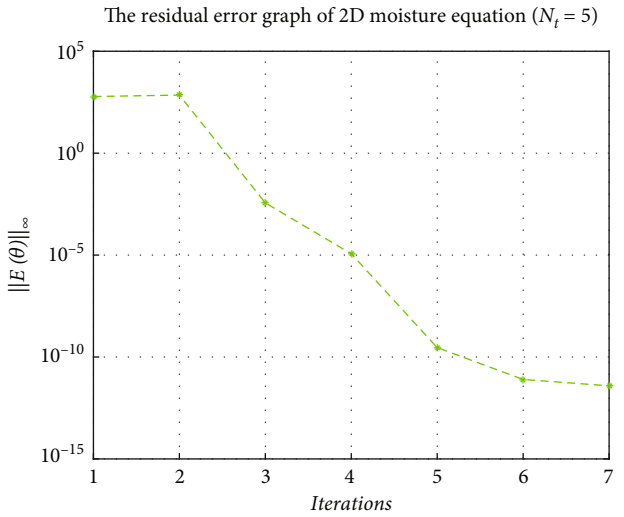

(d) Moisture equation

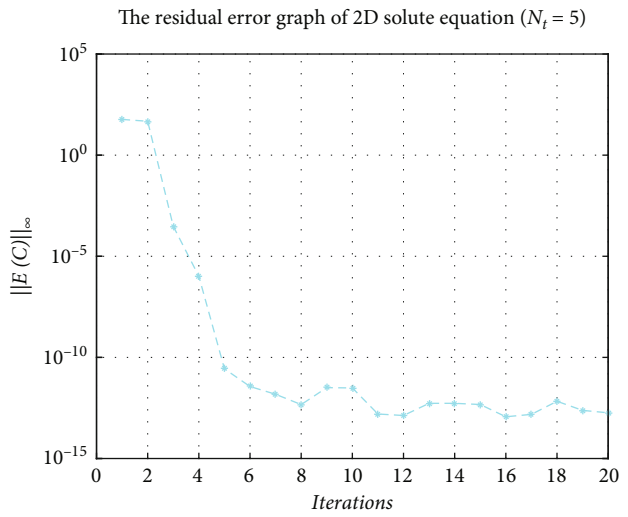

(e) Solute equation

Figure 7: Error norms at different iteration points of the model, for $N_x = N_z = 25$ and $N_t = 5$.

Table 3: Comparing running time and matrix coefficient condition number of the proposed method and the TV-SCM [84] and MV-SQLM [72] for problem, equations (10)–(13) and (19); $N_x = N_z = 20$, $N_t = 5$, and $It = 20$.

T	MV-SLQLM		TV-SCM [84]		MV-SQLM [72]	
	0.5	1.0	0.5	1.0	0.5	1.0
CPU time (sec)	0.21053	0.23741	1.32447	1.463282	0.48465	0.45792
Condition number	1.1804×10^4	1.3548×10^4	3.34237×10^6	3.43821×10^6	2.4567×10^4	2.5045×10^4

Unlike in porous channel (single-phase flow) studies, Figure 8(b) shows that the velocity profile decreases with an increase in Re_p. The reason is that the velocity distribution decreases to satisfy the conservation of pore momentum as Re_p increases because of the condensation process (Figure 1(b)) that occurs at a low Re_p number, consistent with [102]. In addition, in agreement with [102], Figure 8(b) shows that the velocity decay rate is slower at high Re_p than at low Re_p. Moreover, for liquid flows in porous media such as soil, the Reynolds number is generally low, leading to more occurrence of the condensation process.

4.2.2. Heat Distribution. In [92], it was claimed that the local thermal equilibrium in a porous medium becomes stronger as anyone of Re_p, Pr, or the Λ decreases, or the Nusselt number Nu increases. Therefore, we also investigated the effect of Pr and Λ in addition to Ec on the soil temperature distribution profile. Figure 9 shows the variation in temperature profile for varied values of the Prandtl number, Reynolds number, and heat generation/absorption parameter.

Figure 9(a) shows that the heat distribution profile advances at greater values of Re_p, consistent with [102]. When [94] studied the effect of porosity on natural convection of moderate Prandtl number fluids ($\mathrm{Pr} \geq 1$) in a porous medium, heat transfer rate increased with porosity. The reason is that higher porosity leads to a larger contact surface area, thereby intensifying the heat transfer process. However, even at the moderate Prandtl number of 5.2, the heat transfer profiles insignificantly changes at increasing values of ϕ. We therefore do not include its result here. Despite the case, the constant increased values of heat transfer at higher porosity values could be that, for moderately high Prandtl number fluids in porous media, Nu increases nearly linearly with ϕ [94]. The linear relationship between Nu and ϕ, as reported in [94], could explain the observed insignificant changes but at high-temperature values.

The Prandtl number Pr is the ratio of momentum to thermal diffusivity. Figure 9(b) shows the effect of Pr on the temperature distribution profile. Since Pr is inversely proportional to thermal conductivity, several studies indicate that enhancing the Prandtl number causes a decline in the thermal profile because high estimates of the Prandtl number mean weaker thermal diffusivity. Hence, heat diffuses gradually and thus affecting the temperature. However, in the current numerical simulations, soil temperature profiles increase with Prandtl number because the heat transfer characteristics are now influenced by several interactive variables inside the natural convection-dominated porous zone (Figure 1(b)). For heat and mass transfer characteristics of natural convection of large Prandtl number $(1 \leq \mathrm{Pr} \leq 200)$ fluids in porous media such as soil, a recent study found that there exist three characteristic heat transfer zones where the Nusselt number Nu (ratio of heat convection to conduction) depends on Pr monotonically [94]. In particular, [94] found that Nu increases with Pr monotonically for moderate $(1 \leq \mathrm{Pr} \leq 30)$ Prandtl number fluids but decreases in the $(30 < \mathrm{Pr} \leq 140)$ zone and slightly increases again for $\mathrm{Pr} > 140$. Therefore, with reference to the zone of Pr values (Figure 9(b)), soil heat increases with Pr due to the enhanced Nu for natural convection flow [92].

Eckert number Ec characterizes the influence of self-heating of fluid as a consequence of dissipation effects due to internal friction of the fluid. However, in the current study, varying values of Ec did not show any significant effect on the temperature profiles. Therefore, in the current investigated porous domain (Figure 1(b)), the effects of self-heating due to dissipation are negligible. However, under effect of the heat generation/absorption parameter δ_1, the temperature profile increases (Figure 9(c)), where $\delta > 0$ means a heat generation and $\delta_1 < 0$ means a heat absorption, because heat generation escalates the spread and distribution of the temperature. With heat absorption, on the other hand, the temperature of the fluid begins to decline. Hence, the response to the negative temperature gradient from the heat absorption to the heat generation mechanism results in a high thermal diffusion that makes the temperature of the boundary layer rise, leading to a rise in the temperature distribution of the fluid. Finally, we also investigated the effect of varying values of Darcy numbers Λ on temperature profiles. Unfortunately, like a case of porosity ϕ that monotonically depends on permeability k, temperature distribution profiles do not significantly change with Darcy numbers.

4.2.3. Moisture Distribution. As demonstrated by several studies, changes in retardation, temperature gradient, diffusivity ratio, and sink can alter moisture transfer characteristics through the porous medium. Figure 10 shows the effect of varying ϕ, R_n, δ_2, and Le' on changes to moisture distribution. We chose these parameters because, elsewhere, they showed to be sensitive to calculating moisture content.

At varying values of ϕ, moisture distribution profile does not significantly change with porosity (Figure 10(a)). The result correlates with nonsignificant changes to temperature profiles at varying ϕ since increasing porosity enhances evaporation rate, which may lead to reduced moisture content. But, at low Prandtl and Eckert numbers (minimal heat effect), Figure 10(b) shows that soil moisture profiles decrease with an increase in retardation R_n, attributed to

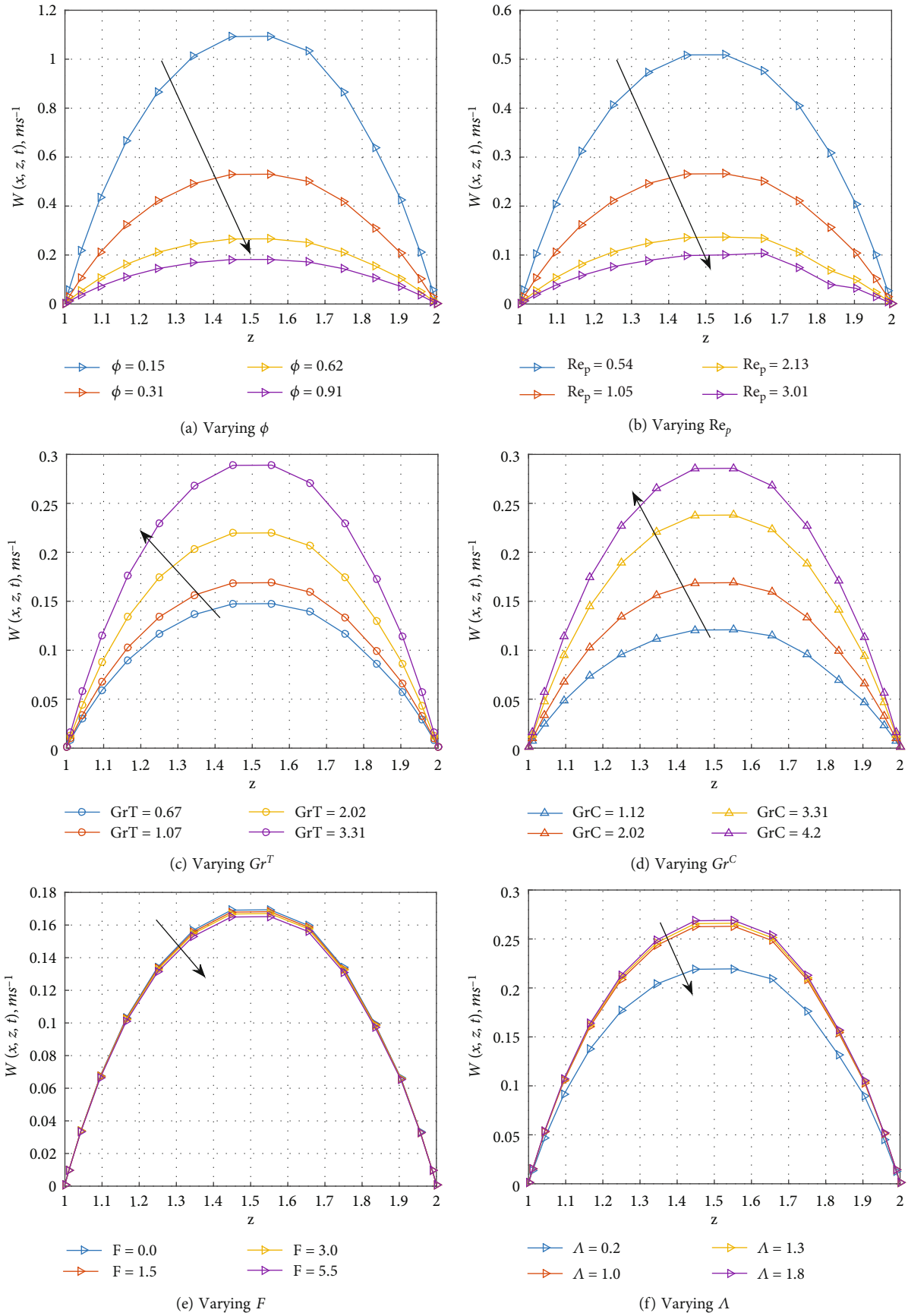

(a) Varying ϕ

(b) Varying Re_p

(c) Varying Gr^T

(d) Varying Gr^C

(e) Varying F

(f) Varying Λ

Figure 8: Effect of ϕ, Re_p, Gr^T, Gr^C, F, and Λ on vertical velocity flow profile.

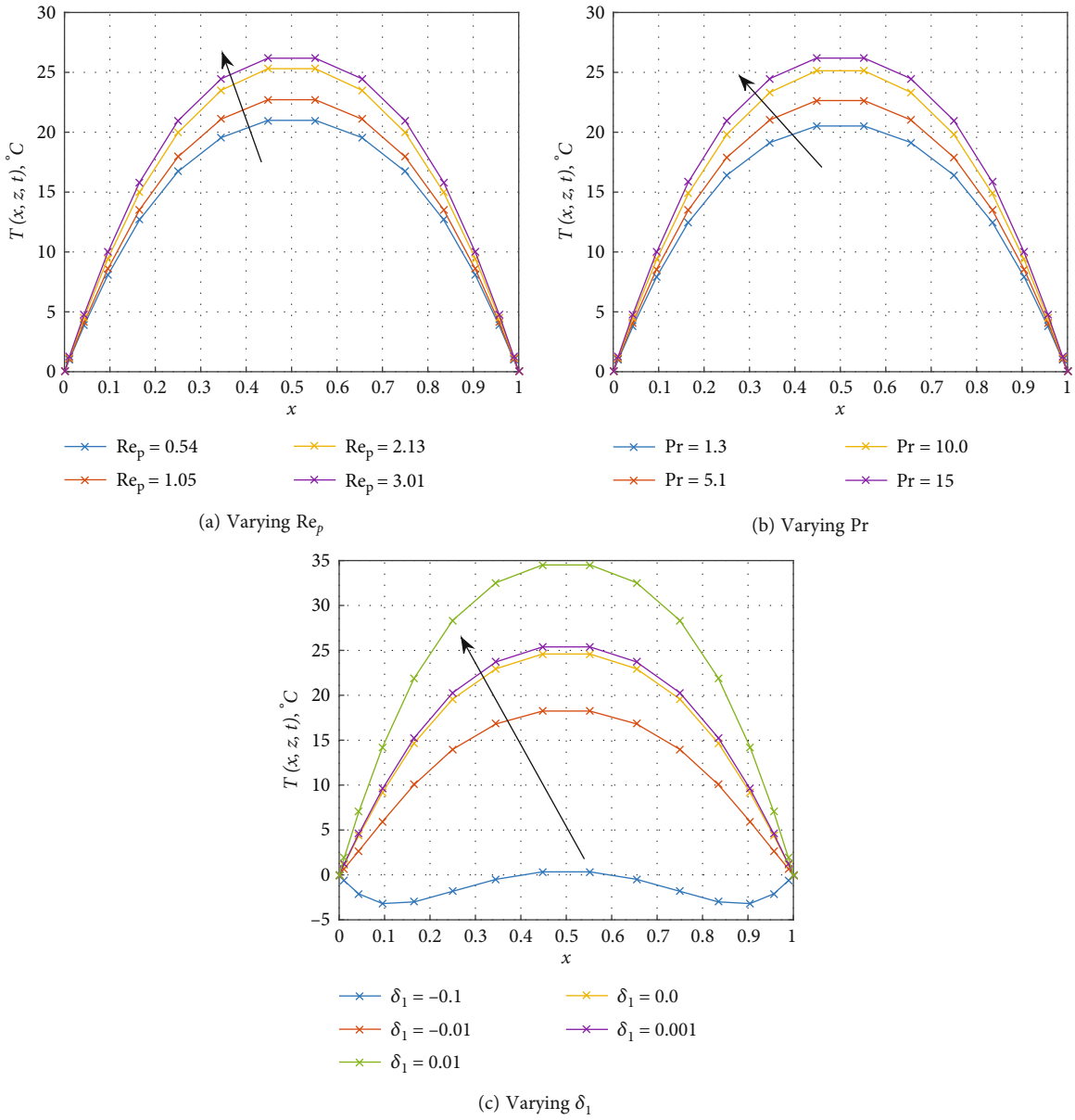

(a) Varying Re_p

(b) Varying Pr

(c) Varying δ_1

FIGURE 9: Effect of Re_p, Pr, and δ_1 on soil temperature profile.

the sink effect when the plant-root uptake mechanism has a significant impact on retardation factor. Consistent with the previous studies, Figure 10(c) shows that moisture profiles decrease with the increasing values of δ_2 due to the redistribution process [25, 103] and low values of isothermal moisture diffusivity D_θ. Using $Le' = D_T/D_\theta$, Figure 10(d) shows the effect of thermal moisture diffusivity D_T on moisture profile in the investigated domain under combined moisture and temperature gradients. Numerical simulations show that for high Le', the evaporation rate is very marginal, leading to a significant impact on moisture content.

4.2.4. Solute Concentration Distribution. Using analytical or semianalytical solutions, studies have shown that solute concentration profiles get affected by the changes in several model parameters, including Pe, $\bar{\zeta}$, and θ_w. In addition, [23] observed the changes in the solute transfer characteristics with the chemical reaction parameter by varying the Damköhler number Da. Similarly, the effect of reaction and absorption coefficients on solute concentration was investigated, respectively, using the deduced "apparent" Damköhler ρ'_3 and "weighted" Damköhler ρ'_4 numbers. However, we specifically observed the effects of varying Da and κ_d present in ρ'_3 and ρ'_4, respectively. To investigate the effect of plant-root uptake activity, the effect of varying the sink coefficient ζ_s was observed. The effect of soil temperatures on solute distribution was investigated by varying the thermophoresis parameter $\bar{\zeta}$. Figure 11 shows the results.

Figure 11(a) shows the effect of varying low Peclet numbers $(0 \le \mathrm{Pe} \le 5)$ on the solute concentration at low Re_p and

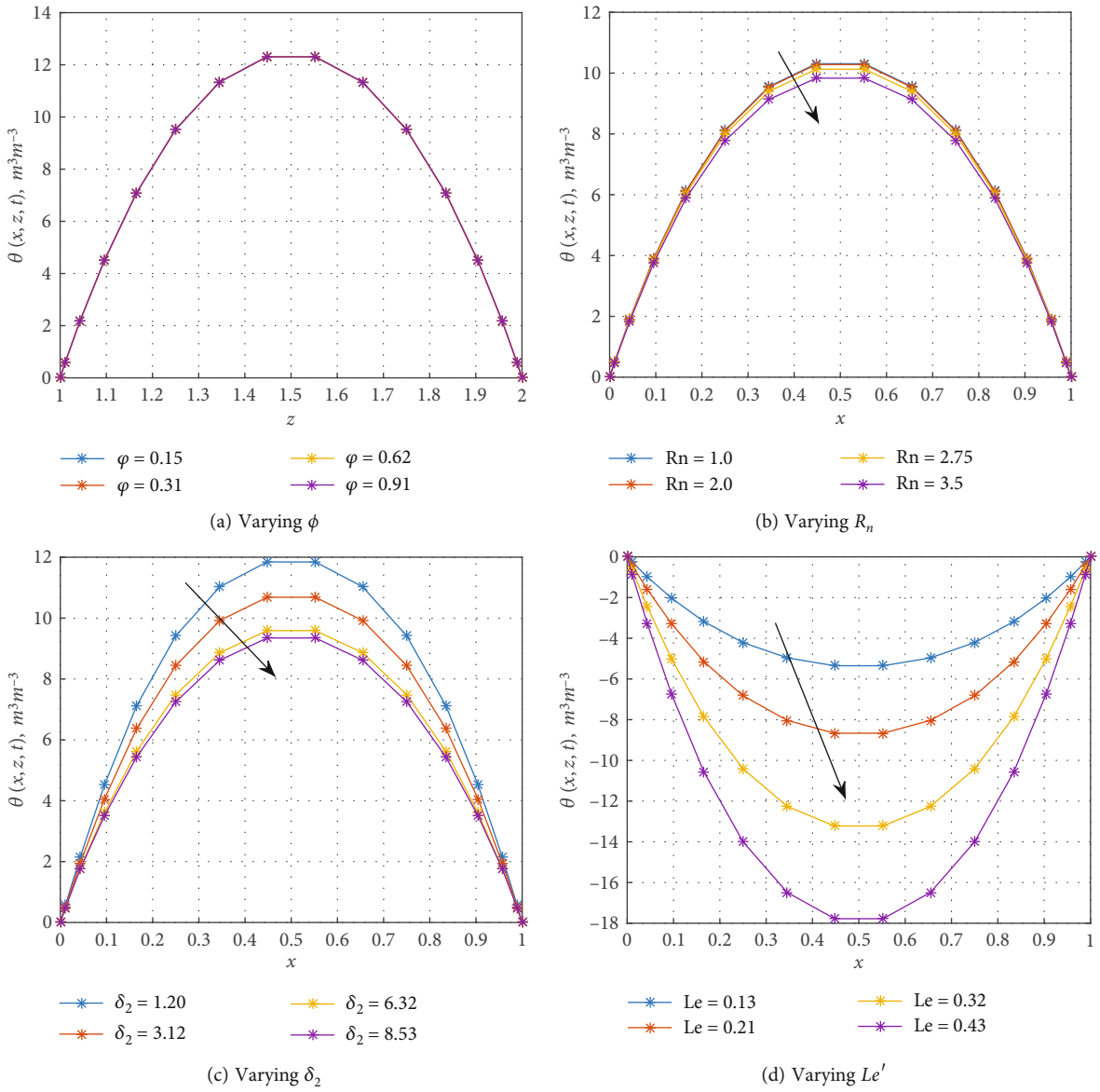

FIGURE 10: Effect of ϕ, R_n, δ_2, and Le' on distribution of moisture.

moderate Da. As mentioned earlier on, we chose the low range of Pe numbers because for the investigated domain that is characterized by laminar flow, diffusion often dominates the transport in the direction perpendicular to the flow streamlines. According to Figure 11(a), solute concentration is generally low at low Peclet numbers with more impact from small than higher Pe values. The reason is that high Pe values, as characterized by the increase in flow velocity or diameter of pore size, tend to enhance the distribution. Since the "apparent" chemical sink parameter $\acute{\varrho}_5$ largely depends on ζ_s (see, equation (29)), the effect of ζ_s on the solute concentration is investigated, and Figure 11(b) shows the results. As expected, solute concentration decreases for an increase in sink parameters, attributed to the plant-root uptake process.

Regarding the change that occurs in the concentration of solute distribution, in the case of the effect of the thermophoresis parameter $\bar{\zeta}$, Figure 11(c) shows that escalation in the values of $\bar{\zeta}$ leads to a higher concentration of the solute distribution in the natural convection zone. The reason is that with an increase in the thermophoresis coefficient, transport force due to the presence of temperature gradient increases, leading to the transfer of more solute particles from the boundary layer region to the cooler region. Hence, by increasing $\bar{\zeta}$, the concentration in the boundary layer decreases, thereby enhancing that of the natural convection zone (cool region). Dejam [23] reported that an increase in Damköhler numbers Da decreases solute concentration because the increased reaction rate leads to a generation of more species. To the contrary, the results of Figure 11(d) show that the distribution of solute concentration increases with Da. The inconsistency arises due to differences in the investigated domain where [23] studied solute transfer in a fractured porous medium.

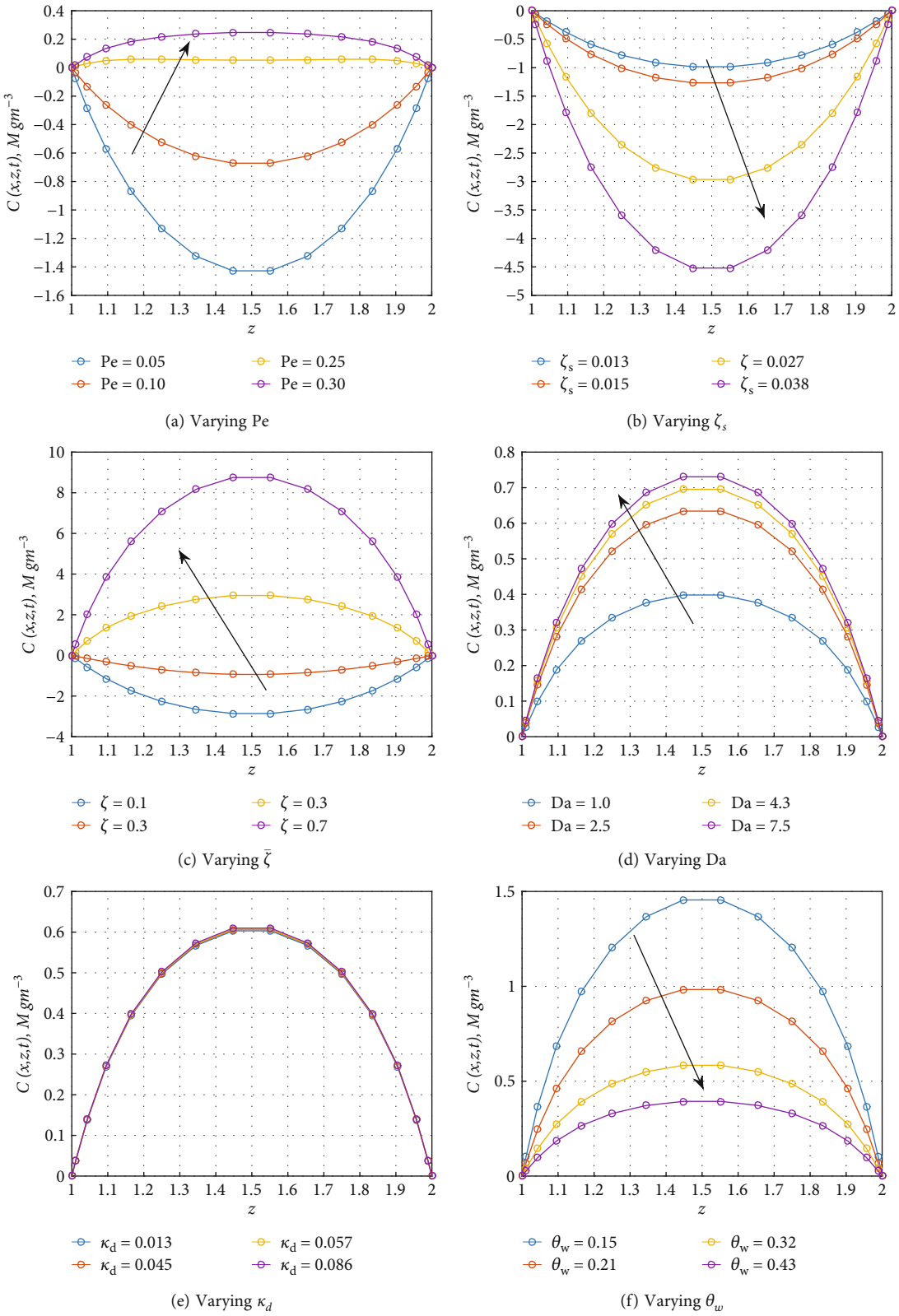

FIGURE 11: Effect of Pe, ζ_s, $\bar{\zeta}$, Da, κ_d, and θ_w on solute concentration profile.

Last but not least, the role of distribution coefficient κ_d in the effect of "weighted" Damköhler number $\acute{\varphi}_4$ (see equation (29)) on the distribution profiles of solute concentration is shown in Figure 11(e). Other studies found that an increase in κ_d decreases solute concentration because increasing κ_d influences the decaying process. In constrast, Figure 11(e)

suggests that when both heat and water contents are present in the media, κ_d insignificantly affects changes of the solute distribution. The reason is that an increase in water content or heat somewhat promotes contact areas, leading to a high rate of solute mixing [104, 105]. Finally, Figure 11(f) shows the effect of varying volumetric water content θ_w on the distribution of solute concentration in which the distribution is low at higher average values of θ_w. The result suggests that the distribution mechanism is now largely facilitated by the increase in dispersion coefficient as the average volumetric water content θ_w reduces [105]. However, it is important to point out that these results are in contrast with other studies. This difference can be attributed to the behavior of molecular diffusion D_w under saturation. Unlike in the unsaturated flow, D_w contributes greatly to the dispersion coefficient because high water contents enhance solute mixing so fast so that the media reaches the Fickian region (equilibrium condition) faster.

5. Conclusions

The purpose of the current study was to propose and apply a multivariate Lagrange polynomial based spectral collocation method to solve a system of coupled nonlinear partial differential equations for modelling transport and interaction of soil moisture, heat, and solute concentration inside a soil ridge when water is present in the furrows. The proposed solution method first uses a quasilinearization method to linearize any nonlinear equations and then employs a local linearization technique to decouple the linearized system of PDEs to form a sequence of equations that are solved in a computationally efficient manner. The applicability of the proposed method, termed the multivariate spectral local quasilinearization method (MV-SLQLM), was demonstrated by the systematic analysis of the effects of varying model parameters on the distribution profiles of velocity, moisture, heat, and solute concentration. The accuracy of the MV-SLQLM solutions on the model was examined through the analysis of residual errors that excellently converge to almost machine precision level. The validity of the approximate numerical results was confirmed against theory and reported findings from the literature. Despite some inconsistencies with the literature, attributed to the physical characteristics of the investigated study domain, the good agreement between the current study findings with those published previously reveals that the proposed numerical scheme is suitable for solving coupled nonlinear PDEs with environmental fluid dynamics applications. Moreover, in comparison, the proposed MV-SLQLM is more efficient than the previous TV-SCM and MV-SQLM at solving large coupled systems of PDEs.

Data Availability

Data sharing not applicable to this article as no datasets were generated or analysed during the current study.

Conflicts of Interest

The authors declare no conflicts of interest.

Acknowledgments

This work was produced as part of PhD study of the corresponding author at Pan African University Institute for Basic Sciences, Technology & Innovation (PAUISTI), funded by the African Union (AU). We are therefore grateful to both AU and PAUISTI.

References

[1] L. Wang, Z. Gao, R. Horton, D. H. Lenschow, K. Meng, and D. B. Jaynes, "An analytical solution to the one-dimensional heat conduction–convection equation in soil," *Soil Science Society of America Journal*, vol. 76, no. 6, pp. 1978–1986, 2012.

[2] Y. Xu, "Similarity solution and heat transfer characteristics for a class of nonlinear convection-diffusion equation with initial value conditions," *Mathematical Problems in Engineering*, vol. 2019, Article ID 3467276, 8 pages, 2019.

[3] Z. Gao, X. Fan, and L. Bian, "An analytical solution to one-dimensional thermal conduction-convection in soil," *Soil Science Society of America Journal*, vol. 168, no. 2, pp. 99–107, 2003.

[4] M. Shao, R. Horton, and D. B. Jaynes, "Analytical solution for one-dimensional heat conduction-convection equation," *Soil Science Society of America Journal*, vol. 62, pp. 123–128, 1998.

[5] J. M. Chen, Y. C. Tan, and C. H. Chen, "Multidimensional infiltration with arbitrary surface fluxes," *Journal of Irrigation and Drainage Engineering*, vol. 127, pp. 370–377, 2001.

[6] J. A. Vrugt, M. T. van Wijk, J. W. Hopmans, and J. Šimunek, "One-, two-, and three-dimensional root water uptake functions for transient modeling," *Water Resources Research*, vol. 37, no. 10, pp. 2457–2470, 2001.

[7] J. M. Chen, Y. C. Tan, and C. H. Chen, "Analytical solutions of one dimensional infiltration before and after ponding," *Hydrological Processes*, vol. 17, no. 4, pp. 815–822, 2003.

[8] A. Sanskrityayn, H. Suk, J. Chen, and E. Park, "Generalized analytical solutions of the advection-dispersion equation with variable flow and transport coefficients," *Sustainability*, vol. 13, no. 14, p. 7796, 2021.

[9] O. Paladino, A. Moranda, M. Massabò, and G. A. Robbins, "Analytical solutions of three-dimensional contaminant transport models with exponential source decay," *Groundwater*, vol. 56, no. 1, pp. 96–108, 2018.

[10] A. Sanskrityayn and N. Kumar, "Analytical solution of advection–diffusion equation in heterogeneous infinite medium using Green's function method," *Journal of Earth System Science*, vol. 125, pp. 1713–1723, 2016.

[11] A. Sanskrityayn, H. Suk, and N. Kumar, "Analytical solutions for solute transport in groundwater and riverine flow using Green's function method and pertinent coordinate transformation method," *Journal of Hydrology*, vol. 547, no. 2, pp. 517–533, 2017.

[12] C. Shan and I. Javandel, "Analytical solutions for solute transport in a vertical aquifer section," *Journal of Contaminant Hydrology*, vol. 27, no. 1–2, pp. 63–82, 1997.

[13] J. Guerrero, L. C. Pimentel, T. Skaggs, and M. Van Genuchten, "Analytical solution of the advection-diffusion transport equation using a change-of-variable and integral transform technique," *International Journal of Heat and Mass Transfer*, vol. 52, no. 13–14, pp. 3297–3304, 2009.

[14] A. Kumar, D. K. Jaiswal, and N. Kumar, "Analytical solutions to one-dimensional advection-diffusion equation with variable coefficients in semi-infinite media," *Journal of Hydrology*, vol. 380, pp. 330–337, 2010.

[15] F. J. Leij and M. T. van Genuchten, "Analytical modeling of nonaqueous phase liquid dissolution with Green's functions," *Transport in Porous Media*, vol. 38, pp. 141–166, 2000.

[16] C. Liu, J. E. Szecsody, J. M. Zachara, and W. P. Ball, "Use of the generalized integral transform method for solving equations of solute transport in porous media," *Advanced Water Resources*, vol. 23, pp. 483–492, 2000.

[17] A. Moranda, R. Cianci, and O. Paladino, "Analytical solutions of one-dimensional contaminant transport in soils with source production-decay," *Soil System*, vol. 2, no. 3, p. 40, 2018.

[18] M. K. Singh, V. P. Singh, P. Singh, and D. Shukla, "Analytical solution for conservative solute transport in one-dimensional homogeneous porous formations with time-dependent velocity," *Journal of Engineering Mechanics*, vol. 135, no. 9, pp. 1015–1021, 2009.

[19] K. Zamani and F. A. Bombardelli, "Analytical solutions of nonlinear and variable-parameter transport equations for verification of numerical solvers," *Environmental Fluid Mechanics*, vol. 14, pp. 711–742, 2014.

[20] F. T. Tracy, "Clean two- and three-dimensional analytical solutions of Richards' equation for testing numerical solvers," *Water Resources Research*, vol. 42, no. 8, 2006.

[21] V. A. Zlotnik, T. Wang, J. L. Nieber, and J. Šimunek, "Verification of numerical solutions of the Richards equation using a traveling wave solution," *Advances in Water Resources*, vol. 30, no. 9, pp. 1973–1980, 2007.

[22] G. Gao, H. Zhan, S. Feng, B. Fu, Y. Ma, and G. Huang, "A new mobile-immobile model for reactive solute transport with scale-dependent dispersion," *Water Resources Research*, vol. 46, no. 8, pp. 1–16, 2010.

[23] M. Dejam, "Advective-diffusive-reactive solute transport due to non-Newtonian fluid flows in a fracture surrounded by a tight porous medium," *International Journal of Heat and Mass Transfer*, vol. 128, pp. 1307–1321, 2019.

[24] H. Suk, "Semi-analytical solution of land-derived solute transport under tidal fluctuation in a confined aquifer," *Journal of Hydrology*, vol. 554, pp. 517–531, 2017.

[25] S. G. Fityus and D. W. Smith, "Solution of the unsaturated soil moisture equation using repeated transforms," *International Journal for Numerical and Analytical Methods in Geomechanics*, vol. 25, pp. 1501–1524, 2001.

[26] V. Novák and H. Hlaváčiková, "Modelling of water flow and solute transport in soil," in *Applied Soil Hydrology*, pp. 319–337, Springer, Cham, Switzerland, 2019.

[27] M. Ehrhardt and R. E. Mickens, "A non-standard finite difference scheme for convection-diffusion equations having constant coefficients," *Applied Mathematics and Computation*, vol. 219, no. 12, pp. 6591–6604, 2013.

[28] L. Wang and L. I. W. Roeger, "Non-standard finite difference schemes for a class of generalized convectiondiffusion-reaction equations," *Numerical Methods Partial Differential Equations*, vol. 31, no. 4, pp. 1288–1309, 2015.

[29] A. Soko, J. Okelo, and V. Masanja, "Identification of the time-dependent point source in a system of two coupled two dimension diffusion-advection-reaction equations: application to groundwater pollution source identification," *Global Journal of Pure and Applied Mathematics*, vol. 16, no. 8, pp. 371–394, 2020.

[30] K. Noborio, K. J. McInnes, and J. L. Heilman, "Two-dimensional model for water, heat, and solute transport in furrow-irrigated soil: I. Theory," *Soil Science Society of America Journal*, vol. 60, pp. 1001–1009, 1996.

[31] K. Noborio, K. J. McInnes, and J. L. Heilman, "Two-dimensional model for water, heat, and solute transport in furrow-irrigated soil: II. Field evaluation," *Soil Science Society of America Journal*, vol. 60, pp. 1010–1021, 1996.

[32] J. G. Benjamin, A. D. Blaylock, H. J. Brown, and R. M. Cruse, "Ridge tillage effects on simulated water and heat transport," *Soil and Tillage Research*, vol. 18, no. 2-3, pp. 167–180, 1990.

[33] A. Baghlani and J. Nikzad, "Differential quadrature method for two-dimensional unsaturated water flow," *Scientia Iranica*, vol. 25, no. 1, pp. 65–73, 2018.

[34] G. Juncu, A. Nicola, and C. Popa, "Nonlinear multigrid methods for numerical solution of the unsaturated flow equation in two space dimensions," *Transport in Porous Media*, vol. 83, pp. 637–652, 2010.

[35] A. H. Abbas, H. Messaoud, D. Saada, and B. Abdennacer, "Numerical study of laminar natural convection in porous media: Darcy-Brinkman-Forcheimer model," *Energy Procedia*, vol. 74, pp. 77–86, 2015.

[36] T. J. Kelleners, J. Koonce, R. Shillito et al., "Numerical modeling of coupled water flow and heat transport in soil and snow," *Soil Science Society of America Journal*, vol. 80, no. 2, pp. 247–263, 2016.

[37] A. Bennett, *Solving Richards' Equation Via Finite Difference Schemes*, NumerischeMathematik, 2017, http://arbennett.github.io/numerical-methods,/hydrology/2017/12/12/\\\url{richards_eq.html}.

[38] K. Reichardt and L. C. Timm, *Water Redistribution after Infiltration into the Soil*, Springer, Cham, Switzerland, 2020.

[39] R. Ren, J. Ma, Q. Cheng, L. Zheng, X. Guo, and X. Sun, "An investigation into the effects of temperature gradient on the soil water-salt transfer with evaporation," *Water*, vol. 9, no. 7, p. 456, 2017.

[40] F. Cimolin and M. Discacciati, "Navier–Stokes/Forchheimer models for filtration through porous media," *Applied Numerical Mathematics*, vol. 72, pp. 205–224, 2013.

[41] K. Fujisawa and A. Murakami, "Numerical analysis of coupled flows in porous and fluid domains by the Darcy-Brinkman equations," *Soils and Foundations*, vol. 58, pp. 1240–1259, 2018.

[42] M. A. Celia, E. T. Bouloutas, and R. L. Zarba, "A general mass-conservative numerical solution for the unsaturated flow equation," *Water Resources Research*, vol. 26, pp. 1483–1496, 1990.

[43] N. Li, X. Yue, and L. Ren, "Numerical homogenization of the Richards equation for unsaturated water flow through heterogeneous soils," *Water Resources Research*, vol. 52, pp. 8500–8525, 2016.

[44] J. Simunek, M. Sejna, H. Saito, M. Sakai, and M. T. van Genuchten, "The HYDRUS-1D software package for simulating the movement of water, heat, and multiple solutes in variably saturated media, version 4.0, HYDRUS Software Series 3," Technical report for Department of Environmental Sciences, University of California Riverside, 2008, https://www.ars.usda.gov/arsuserfiles/20360500/pdf_pubs/P2119.pdf.

[45] H. Fujimaki, "Determination of irrigation amounts using a numerical model," in *The Third HYDRUS Workshop*, H.

Saito, M. Sakai, N. Toride, and J. Šimunek, Eds., pp. 29–38, Tokyo University of Agriculture and Technology, Tokyo, Japan, 2008.

[46] K. Watanabe, "Water and heat flow in a directionally frozen silty soil," in *The Third HYDRUS Workshop*, H. Saito, M. Sakai, N. Toride, and J. Šimunek, Eds., pp. 20–28, Tokyo University of Agriculture and Technology, Tokyo, Japan, 2008.

[47] S. S. Haile, *VS2DRT: variably saturated two dimensional reactive transport modeling in the vadoze zone, [Ph.D. thesis]*, Faculty of Geosciences - Universität Bergakademie Freiberg, 2013, https://core.ac.uk/download/pdf/235261394.pdf.

[48] E. H. Doha, D. A. H. Bhrawy, R. M. Hafez, and M. A. Abdelkawy, "A Chebyshev-Gauss-Radau scheme for nonlinear hyperbolic system of first order," *Applied Mathematics and Information Science*, vol. 8, 2014.

[49] I. P. Mas, B. A. Hidayat, S. Parman, and S. Irawan, "A meshfree approach for transient heat conduction analysis of nonlinear functionally graded materials," *International Journal of Computational Methods*, vol. 15, no. 2, article 1850007, 2017.

[50] F. X. Giraldo and M. Restelli, "A study of spectral element and discontinuous Galerkin methods for the Navier-Stokes equations in nonhydrostatic mesoscale atmospheric modeling: equation sets and test cases," *Journal of Computational Physics*, vol. 227, no. 8, pp. 3849–3877, 2008.

[51] S. Marras, J. F. Kelly, M. Moragues et al., "A review of element-based Galerkin methods for numerical weather prediction: finite elements, spectral elements, and discontinuous Galerkin," *Archives of Computational Methods in Engineering*, vol. 23, no. 4, pp. 673–722, 2016.

[52] C. Canuto, M. Y. Hussaini, A. Quarteroni, and T. A. Zang, *Spectral Methods in Fluid Dynamics*, Springer-Verlag, New York, NY, USA, 1988.

[53] C. Canuto, Y. M. Hussaini, A. Quarteroni, and T. A. Zang, *Spectral Methods: Fundamentals in Single Domains*, Springer-Verlag, Berlin, 2006.

[54] J. Shen, T. Tang, and L. Wang, *Spectral Methods: Algorithms, Analysis and Applications*, Springer, New York, NY, USA, 2011.

[55] L. N. Trefethen, *Spectral Methods in MATLAB*, SIAM, Philadelphia, PA, USA, 2000.

[56] K. Cheuprasert and N. Kanyamee, "A Chebyshev-Gauss collocation method for the numerical solution of ordinary differential equations," *Songklanakarin Journal of Science and Technology*, vol. 39, pp. 383–397, 2017.

[57] G. I. El-Baghdady and M. S. El-Azab, "Chebyshev-Gauss-Lobatto pseudo-spectral method for one-dimensional advection-diffusion equation with variable coefficients," *Sohag Journal of Mathematics*, vol. 3, no. 1, pp. 7–14, 2016.

[58] A. H. Khater, R. S. Temsah, and M. M. Hassan, "A Chebyshev spectral collocation method for solving Burgers'-type equations," *Journal of Computational and Applied Mathematics*, vol. 222, no. 2, pp. 333–350, 2008.

[59] N. Rai and S. Mondal, "Spectral methods to solve nonlinear problems: a review," *Partial Differential Equations in Applied Mathematics*, vol. 4, article 100043, 2021.

[60] S. S. Motsa, "A new spectral local linearization method for nonlinear boundary layer flow problems," *Journal of Applied Mathematics*, vol. 2013, Article ID 423628, 15 pages, 2013.

[61] S. Motsa, "On the new bivariate local linearisation method for solving coupled partial differential equations in some applications of unsteady fluid flows with heat and mass transfer," in *Mass Transfer -Advancement in Process Modelling*, M. Solecki, Ed., IntechOpen, London, UK, 2015.

[62] T. Thumma and V. M. Magagula, "Transient electromagnetohydrodynamic radiative squeezing flow between two parallel Riga plates using a spectral local linearization approach," *Heat Transfer-Asian Research*, vol. 49, pp. 67–85, 2020.

[63] S. S. Motsa, "On the bivariate spectral homotopy analysis method approach for solving nonlinear evolution partial differential equations," *Abstract and Applied Analysis Journal*, vol. 2014, article 350529, pp. 1–8, 2014.

[64] M. S. Ansari, V. M. Magagula, and M. Trivedi, "Jeffrey nanofluid flow near a Riga plate: spectral quasilinearization approach," *Heat Transfer*, vol. 49, no. 3, pp. 1491–1510, 2020.

[65] V. Magagula, S. Motsa, and P. Sibanda, "Multidomain bivariate pseudo-spectral quasilinearization method for systems of nonlinear partial differential equations," *Methods*, vol. 2, no. 4, 2020.

[66] M. Jamil, A. Baveja, and R. Batta, "Bivariate spectral local linearisation method (BSLLM) for unsteady MHD micropolar-nanofluids with homogeneous-heterogeneous chemical reactions over a stretching surface," *International Journal of Applied and Computational Mathematics*, vol. 5, no. 1, pp. 1–14, 2019.

[67] S. S. Motsa, F. M. Samuel, and S. Shateyi, "Solving nonlinear parabolic partial differential equations using multidomain bivariate spectral collocation method," in *Nonlinear Systems - Design, Analysis, Estimation and Control*, pp. 1–11, IntechOpen, London, UK, 2016.

[68] V. M. Magagula, S. S. Motsa, and P. Sibanda, "A multidomain bivariate pseudospectral method for evolution equations," *International Journal of Computational Methods*, vol. 14, no. 4, article 1750041, 2017.

[69] V. M. Magagula, "On the multidomain bivariate spectral local linearisation method for solving systems of nonsimilar boundary layer partial differential equations," *International Journal of Mathematics and Mathematical Sciences*, vol. 2019, Article ID 6423294, 18 pages, 2019.

[70] V. M. Magagula, S. S. Motsa, and P. Sibanda, "On the bivariate spectral quasilinearization method for nonlinear boundary layer partial differential equations," in *Applications of Heat, Mass and Fluid Boundary Layers*, pp. 177–190, Woodhead Publishing, London, UK, 2020.

[71] M. Mkhatshwa, S. Motsa, and P. Sibanda, "Overlapping multi-domain spectral method for conjugate problems of conduction and MHD free convection flow of nanofluids over flat plates," *Mathematical and Computational Applications*, vol. 24, p. 75, 2019.

[72] G. P. Dlamini and V. Magagula, "A multivariate spectral quasi-linearization method for the solution of (2+1) dimensional Burgers' equations," *International Journal of Nonlinear Sciences and Numerical Simulation*, vol. 21, no. 7-8, pp. 683–691, 2020.

[73] M. Lekoko, S. Oloniiju, and G. Magalakwe, "Analysis of pressure and heat distribution in a dilating or contracting filter chamber with two outlets using multivariate spectral quasilinearization method," *Heat Transfer*, vol. 51, no. 2, pp. 1543–1567, 2021.

[74] S. Goqo, H. Mondal, P. Sibanda, and S. Motsa, "A multivariate spectral quasilinearisation method for entropy generation in a square cavity filled with porous medium saturated by

nanofluid," *Case Studies in Thermal Engineering*, vol. 14, article 100415, 2019.

[75] F. M. Samuel and S. S. Motsa, "Improved trivariate spectral collocation method of solution for two-dimensional nonlinear initial-boundary value problems via domain decomposition," in *Proceedings PACT 2019 University of Swaziland*, Swaziland, Swaziland, 2019.

[76] R. Bellman, R. E. Kalaba, and J. A. Lockett, *Numerical Inversion of the Laplace Transform: Applications to Biology, Economics, Engineering, and Physics*, Elsevier, New York, NY, USA, 1966.

[77] L. J. Bridge, *Condensation in a Porous Medium, [M.S. thesis]*, The University of British Columbia, 2001, https://open.library.ubc.ca/media/download/pdf/831/1.0080047/1/1243.

[78] E. P. Mwakilama, D. K. Gathungu, and V. M. Magagula, *A Two-Dimensional Pseudo-Spectral Scheme for Modelling Heat, Moisture, and Solute Transport in Soil Ridge: Development and Application, [Ph.D. thesis]*, Pan African University Institute for Basic Sciences, Technology, and Innovation, Nairobi, Kenya, 2022.

[79] R. C. Martineau, R. A. Berry, A. Esteve et al., "Comparative analysis of natural convection flows simulated by both the conservation and incompressible forms of the Navier-Stokes equations in a differentially-heated square cavity," Technical Report from Idaho National Laboratory, 2009, https://core.ac.uk/download/pdf/194439928.pdf.

[80] R. Rotz, "Hydrogeologic properties of earth materials and principles of groundwater flow," *Groundwater*, vol. 59, pp. 320-321, 2021.

[81] G. Akgün and H. Kurtaran, "Large displacement transient analysis of FGM super-elliptic shells using GDQ method," *Thin-Walled Structures*, vol. 141, pp. 133–152, 2019.

[82] M. Ilati and M. Dehghan, "Error analysis of a meshless weak form method based on radial point interpolation technique for Sivashinsky equation arising in the alloy solidification problem," *Journal of Computational and Applied Mathematics*, vol. 327, pp. 314–324, 2018.

[83] A. H. Bhrawy, "A highly accurate collocation algorithm for 1 +1 and 2+1 fractional percolation equations," *Journal of Vibration and Control*, vol. 5, pp. 1–23, 2015.

[84] F. M. Samuel and S. S. Motsa, "A highly accurate trivariate spectral collocation method of solution for two- dimensional nonlinear initial-boundary value problems," *Applied Mathematics and Computation*, vol. 360, pp. 221–235, 2019.

[85] N. Karjanto, "Properties of Chebyshev polynomials," *Publication Scientifique de_l AEIF*, vol. 2, pp. 127–132, 2002.

[86] E. Mwakilama, D. Gathungu, and V. Magagula, "Use of variational method to evaluate well-posedness of an advection-diffusion reaction equation of solute transport," *Applied Mathematical Sciences*, vol. 16, no. 7, pp. 313–327, 2022.

[87] B. Yu, W. Q. Tao, D. S. Zhang, and Q. W. Wang, "Discussion on numerical stability and boundedness of convective discretized scheme," *Numerical Heat Transfer, Part B: Fundamentals: An International Journal of Computation and Methodology*, vol. 40, no. 4, pp. 343–365, 2001.

[88] R. Corless and S. Watt, "Bernstein bases are optimal, but, sometimes, Lagrange bases are better," 2004, https://www.csd.uwo.ca/~watt/pub/reprints/2004-synasc-lagrange.pdf.

[89] J. M. Carnicer, Y. Khiar, and J. M. Peña, "Optimal stability of the Lagrange formula and conditioning of the newton formula," *Journal of Approximation Theory*, vol. 238, pp. 52–66, 2019.

[90] A. Abdullah, "Mathematical relationship between grid and low Peclet numbers for the solution of convection-diffusion equation," *Journal of Engineering and Applied Sciences*, vol. 13, no. 9, pp. 382–387, 2018.

[91] L. A. Barba and G. F. Forsyth, "CFD python: the 12 steps to Navier-Stokes equations," *Journal of Open Source Education*, vol. 1, no. 9, p. 21, 2018.

[92] J. K. Sung and P. J. Seok, "Effects of the Darcy number, the Prandtl number, and the Reynolds number on local thermal non-equilibrium," *International Journal of Heat and Mass Transfer*, vol. 45, pp. 3885–3896, 2002.

[93] K. Murali, V. Kesavulu, and B. Venkatesh, "Solution of Darcy-Brinkman-Forchheimer equation for irregular flow channel by finite elements approach," *Journal of Physics: Conference Series*, vol. 1172, article 012033, 2019.

[94] S. Chen, W. Li, and H. I. Mohammed, "Heat transfer of large Prandtl number fluids in porous media by a new lattice Boltzmann model," *International Communications in Heat and Mass Transfer*, vol. 122, article 105129, 2021.

[95] T. Hayat, S. Qayyum, S. A. Shehzad, and A. A. Ahmed, "Chemical reaction and heat generation/absorption aspects in flow of Walters-B nanofluid with Cattaneo-Christov double-diffusion," *Results in Physics*, vol. 7, pp. 4145–4152, 2017.

[96] M. Huysmans and A. Dassargues, "Review of the use of Peclet numbers to determine the relative importance of advection and diffusion in low permeability environments," *Hydrogeology Journal*, vol. 13, pp. 895–904, 2005.

[97] L. Xu, J. Yang, Q. Zhang, and H. Niu, "Modelling water and salt transport in a soil–water–plant system under different groundwater tables," *Journal of Taibah University for Science*, vol. 22, pp. 265–273, 2008.

[98] J. Ren, W. Zhang, J. Yang et al., "A comparison of numerical and Lu modeling of water flow and heat transport with laboratory experiments," *Environment and Earth Science*, vol. 78, no. 8, pp. 118–126, 2019.

[99] M. Inoue, J. Simunek, S. Shiozawa, and J. W. Hopmans, "Simultaneous estimation of soil hydraulic and solute transport parameters from transient infiltration experiments," *Advances in Water Resources*, vol. 23, pp. 677–688, 2000.

[100] J. L. Monteith, "Transport of heat, mass, and momentum," in *Principles of Environmental Physics*, pp. 25–35, Springer, Canada, 2013.

[101] M. M. Rahman, R. Liedl, and P. Grathwohl, "Sorption kinetics during macropore transport of organic contaminants in soils: laboratory experiments and analytical modeling," *Water Resources Research*, vol. 40, no. 1, 2004.

[102] J. Cha, S. Lim, T. Kim, and W. G. Shin, "The effect of the Reynolds number on the velocity and temperature distributions of a turbulent condensing jet," *International Journal of Heat and Fluid Flow*, vol. 67, pp. 125–132, 2017.

[103] R. D. Stewart, D. E. Rupp, M. R. Abou-Najm, and J. S. Selker, "Modelling effect of initial soil moisture on sorptivity and infiltration," *Water Resources Research*, vol. 49, pp. 7037–7047, 2013.

[104] S. A. Hosseini and M. Javadimehr, "The effect of temperature variation on radio iodine adsorption in soils," *Asian Journal of Applied Sciences*, vol. 4, no. 4, pp. 439–446, 2011.

[105] I. Y. Padilla, T. C. Jim-Yeh, and M. H. Conklin, "The effect of water content on solute transport in unsaturated porous media," *Water Resources Research*, vol. 35, pp. 3303–3313, 1999.